LA-UR-24-31870

Approved for public release; distribution is unlimited.

Title: The mechanical properties of Kel-F 800 (FK-800) as a function of crystallinity

Author(s): Rae, Philip John

Intended for: Report

Issued: 2024-11-04

Los Alamos
NATIONAL LABORATORY

Los Alamos National Laboratory, an affirmative action/equal opportunity employer, is operated by Triad National Security, LLC for the National Nuclear Security Administration of U.S. Department of Energy under contract 89233218CNA000001. By approving this article, the publisher recognizes that the U.S. Government retains nonexclusive, royalty-free license to publish or reproduce the published form of this contribution, or to allow others to do so, for U.S. Government purposes. Los Alamos National Laboratory requests that the publisher identify this article as work performed under the auspices of the U.S. Department of Energy. Los Alamos National Laboratory strongly supports academic freedom and a researcher's right to publish; as an institution, however, the Laboratory does not endorse the viewpoint of a publication or guarantee its technical correctness.

The mechanical properties of Kel-F 800 (FK-800) as a function of crystallinity

Philip Rae, Los Alamos National Laboratory, Los Alamos, NM 87545

History

Kel-F 800 is a copolymer of chlorotrifluoroethylene PTFE (75 wt. %) and vinylidene fluoride PVDF (25 wt. %)[1]. It has previously been used as a PBX binder for insensitive explosives such as PBX 9502 and LX-17. 3M started production of Kel-F 800 in 1957 and small-scale batches continued to be made until 2002 when production ceased due to environmental concerns regarding one of the emulsifiers used during production. Around 2000 the Kel-F 800 name was changed to FK-800 to avoid trademark concerns because rights to produce another polymer with a similar tradename (Kel-F 81) had been sold to another manufacturer. The Kel designation came from the original manufacturer of PCTFE (Kel-F 81), the Kellog company. To avoid confusion this document will only refer to Kel-F 800. In 2006, production of small-scale batches of Kel-F 800 was started again by 3M in response to customer enquiries. This new material, the first blended batch is referred to as LOT 1, was produced with a different emulsifier than used previously.

Because Kel-F 800 is made in a small batch reactor, considerable variation in crystallinity can be expected from lot to lot and year to year. In many ways, this is not significant since the material is dissolved in a solvent (often MEK, ethylmethyl ketone or ethyl acetate) for PBX production purposes. This destroys the as received crystallinity and the resulting crystallinity in the processed material is a function of polymer molecular weight and thermal history. Producing large billets of Kel-F 800 from solvent extraction is not practical and so a compression molding technique has been used above the melting temperature. This method also removes residual crystallinity from the supplied granules.

The molecular weight of a polymer can be estimated by several techniques, the most common being gel permittivity chromatography (GPC), size exclusion chromatography (SEC)[2] and shear rheometry measurements of polymer/solvent solutions[3]. Changes in molecular weight will affect the crystallization rate and the maximum crystallinity reached for a specific thermal history. Both references [2, 3] agree that the new LOT 1 material molecular weight falls within the deviation found from averaging previous historical lots of Kel-F 800.

Polymer Bonded Explosive Production

This report primarily deals with the application of Kel-F 800 to polymer-bonded explosives (PBXs). It therefore makes sense to study the properties of the material under conditions similar to those resulting from the production process and subsequent thermal annealing in use. Figure 1 shows a flow diagram of the key Kel-F 800 steps involved in producing PBX 9502, an explosive that uses Kel-F 800 as a binder.

It is supposed that dissolving a polymer in a solvent destroys all crystallinity but leaves the molecular weight relatively unchanged. After precipitating the polymer onto the explosive crystals the drying period at 65˚C will re-introduce some level of

crystallinity (annealing well above the T_g of ~27˚C). This crystallinity should then be removed again by heating the polymer well above the melting temperature for several hours. The final cooling period will allow some crystallinity to be formed.

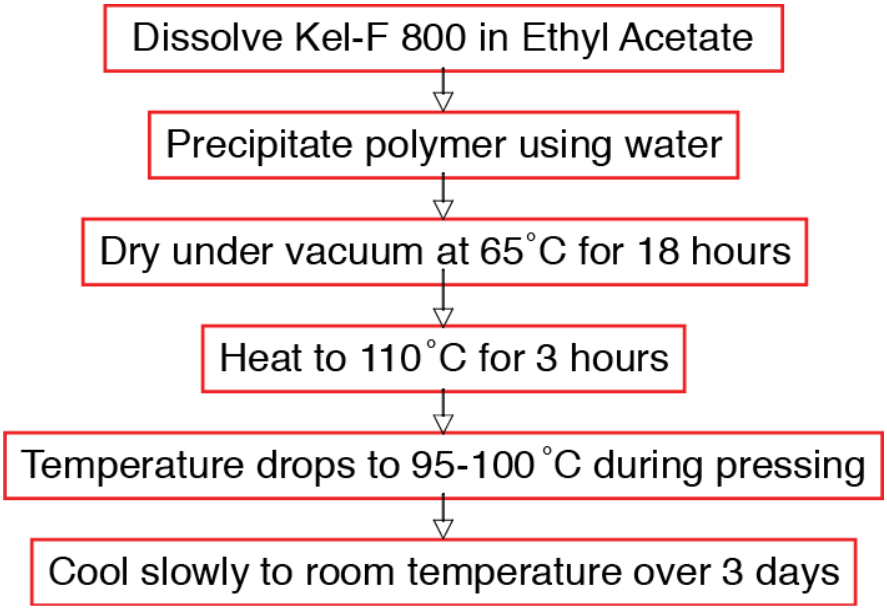

Figure 1. The key steps in the production of PBX 9502 with respect to the Kel-F 800 binder component.

To test this theory, material from lot 30013 was subjected to a thermally simulated production process involving dissolving the polymer, precipitating it, drying, melting and slow cooling over three days. For comparison a sample was cut from an Afton Plastics processed billet and melted and annealed in the same oven as the precipitated sample. At each stage, a sample was removed and stored for subsequent DSC analysis.

In figure 2 the results of the DSC analysis are presented. The curves have been arbitrarily shifted in the y-axis to aid discrimination. It will be noted that the as-precipitated material has a considerable water content evidenced by the 0˚C endotherm. Drying at 65˚C introduces a sizable single crystallinity peak that disappears after melting at 110˚C. This is also true for the billet material also subjected to melting. After slow cooling from 100˚C to room temperature over 3 days both the precipitated material and the billet exhibit similar levels of crystallinity with the value for the precipitated material being a slightly higher. The slow cooling process produces a double melt endotherm rather than the single one seen after annealing at 65˚C.

PBX 9502 returned from the stockpile will have been subjected to some level of thermal annealing. To simulate this an annealing temperature of 40˚C was chosen. Therefore, it seemed sensible to study Kel-F 800 in some detail at two crystallinity states. The first reflects the properties just after production when the crystallinity would be approximately 5%. Serendipitously, this was very similar to the crystallinity of one of the

billets produced by Afton Plastics. The second state was material with a 5% starting crystallinity subjected to prolonged annealing at 40˚C.

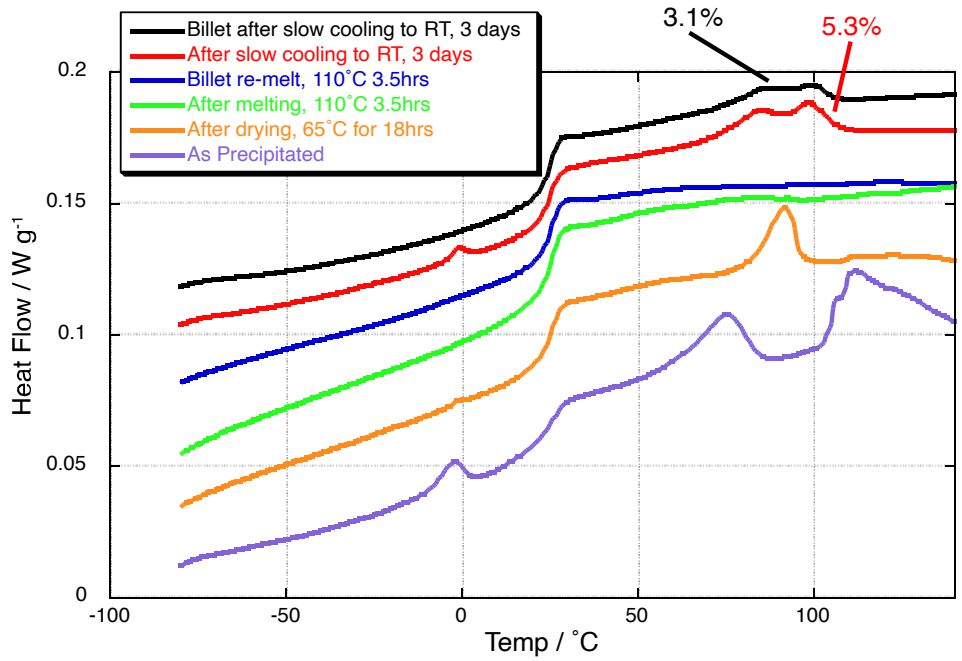

Figure 2. DSC traces from samples removed from a simulated production process for PBX 9502 with respect to the Kel-F 800 binder.

Experimental

Billets of Kel-F 800 were compression molded by Afton Plastics (www.aftonplastics.com). The billets were approximately 150 mm×150 mm×50 mm. The material was processed according to the following two-stage schedule. 1) Heat to 125˚C for 4 hours prior to pressing with 20 tons. This stage forces out most of the bubbles formed from material outgassing. 2) after a further 4-4.5 hours at the same temperature, press with 45 tons in room air holding for two hours. After pressing, remove from mold and continue cooling to ambient temperature. The crystallinity of one of the billets was measured using the DSC method and found to be 2.1%. This compares to 5.0% measured on a previous billet of Kel-F 8001 prepared in an identical fashion[1]. To try to increase the crystallinity to a similar level, the LOT 1 billet was placed in an oven at 65˚C for 8 hours. The end state crystallinity measured a little higher than desired at 7.4%. Despite this, the billet was machined for mechanical testing.

Differential Scanning Calorimetry (DSC) was performed on a TA Instruments Q2000 Modulated Differential Scanning Calorimeter. A helium purge was utilized with a flow rate of 25 mL min^{-1}. The temperature was controlled using a liquid nitrogen cooling accessory. The samples were encapsulated in aluminum Tzero® pans. The instrument was calibrated with indium and sapphire standards. The DSC scans were run at 10˚C min^{-1} heating rate from -100˚C. The melting temperature is defined as the peak in

[1] 3M reference 98-0210-1002-4, lot 30013 manufactured Nov 2001

the melting endotherm and for Kel-F 800, the crystallinity is defined as the area under the melting endotherm divided by the melt endotherm of fully crystalline PCTFE (43.5 J/g) [4]. This value of melting endotherm is somewhat contentious because it is a value for the major homopolymer constituent in Kel-F 800 but it is unclear that the addition of the second constituent in a random fashion on the backbone and the resulting disruption will not significantly alter this value. Nevertheless, historically the value for PCTFE has been used and this document will follow this tradition. The glass transition temperature is defined as the midpoint of the heat flow of the step transition.

The dynamic mechanical properties of the samples were measured on a TA Instruments Q800 Dynamic Mechanical Analyzer (DMA) with liquid nitrogen cooling accessory. The samples were run in tensile geometry. The samples were machined from a pressed billet and had dimensions approximately 2 mm thickness, 10 mm width and 12 mm in length. The samples were measured at frequencies between 0.1 and 100 Hz to a strain of 0.1%. After a frequency sweep was completed, the temperature was increased by 2˚C and another frequency sweep was run.

Given the ductile nature of the polymers, samples were deformed to large strains in many cases. For this reason, all strains referenced in this document, unless otherwise noted, are true-strains (logarithmic strains). A constant loading strain-rate was maintained for all large-strain compression experiments. The feedback loop from the testing machines was closed to correctly slow the crosshead as the samples thinned. True-stress was calculated assuming a constant sample volume. The compression sample geometry chosen was 6.375 mm diameter by 6.375 mm long right-regular cylinders. The aspect ratio of 1.1 is smaller than the 1.1.5-1.2 values often employed in compression tests on metals, but the sample size and ratio was chosen to conserve material for the large number of tests required and prevent the trapezoidal shearing deformation mode observed in some soft polymers.

For the compression tests, both an MTS 880 and MTS 810 servo-hydraulic machines were utilized. These machines ran MTS TestStar software also allowing for full control over the test profile. For all samples tested at -20˚C, or higher, paraffin wax was used to lubricate the specimen ends [5, 6]. The specimens were compressed between highly polished tungsten carbide platens to further lower the friction. Temperature control was carried out using either electrically heated or liquid nitrogen cooled platens and surrounding insulation was used to create a small environmental chamber. The samples were allowed to equilibrate at temperature for between 30 and 45 minutes prior to testing.

For the tensile experiments, a screw driven Instron 4482 frame was used. This machine has been fitted with a modern PC control system (MTS Testworks 4) allowing a wide range of control modes and input channels. Samples were machined to form ASTM D-638 Type V specimens. All specimens were allowed to equilibrate at the testing temperature for between 45 and 100 minutes prior to tensile testing. At room temperature, both materials have a large strain to failure (>500% engineering strain). Measuring these large displacements accurately is challenging. The method chosen for this study was a Messphysik ME-46 video extensometer. This device uses a black and white CCD camera to digitally capture as a function of time an image of the deforming sample, upon which fiducial markers have been attached. Using a sophisticated real-time

correlation algorithm, the distance between the markers can be continuously measured. In this way, a non-contacting measurement of strain can be made to large values (>1000%). Several methods of affixing the fiducials were tried, the most effective method was to use wires held in place by small rubber `O'-rings. By back-lighting the sample, a high contrast image about the wires was created and whilst the `O'-rings deformed with the sample, the wires did not slip. At high or low temperatures (>50˚C or <0˚C) the `O'-rings were unsatisfactory and small metal springs were used. The ME-46 is equipped with an analogue voltage output that is proportional to the measured strain. This voltage was fed into the testing machine, correctly scaled, and used to close the feedback crosshead-rate loop.

For high strain-rate compression testing (2000-3000 s^{-1}), a LANL-built split-Hopkinson pressure bar was used [7]. This Hopkinson bar is fitted with a small environmental chamber surrounding the test sample. In the chamber, either heated or cooled gas can be introduced to vary the sample temperature between -100 and +200˚C. The change in impedance at the ends of the Ti-6Al-4V bars used for testing in this temperature range is negligible. As before, paraffin wax was used to lubricate the specimen ends for all samples tested at -20˚C or higher. No lubricant was used at lower temperatures, but owing to the relatively small strains imposed on the sample and the low coefficient of friction between the material and the finely finished pressure bars, no sample barreling was found.

The Taylor test was developed by G. I. Taylor shortly after World War II as a method of estimating the dynamic yield strength of metals. It involves shooting a small right cylindrical test specimen at an ‘infinite’ steel block. From post-test analysis, information about the samples dynamic mechanical response can be generated. The test is still in use but is now mostly used as a verification of a computational computer codes predications of dynamic material response. Taylor impact cylinders were machined from the plate with dimensions of 7.62 mm diameter by 38.1 mm long. Rods were fired at velocities between 105 & 202 m/s and temperatures of 23 and 60˚C. An Imacon 200 high-speed framing camera coupled to a Cordin 463 proportional delay generator was used to record back-lit images of the impacts. In all cases a 350 ns exposure was used and 16 frames were recorded with 15μs inter-frame time. The system has been more fully described elsewhere [8].

Reference Billet Results

The majority of the research reported in this document was undertaken on the 3M lot 30013. This lot was purchased to form the LANL strategic stockpile in case more PBX 9502 needs to be produced in the future. Since all new PBX 9502 will be made from this exact material is makes sense to understand its specific properties.

A billet of Afton Plastics compression molded material was sent for machining into a number of specimen geometries. This billet had an as received crystallinity of approximately 5%. Samples for DMA, tension, compression, fracture toughness and Taylor impact testing were obtained. The tensile and compressive response as a function of strain-rate and temperature will be discussed here.

Figure 3 shows the compressive response as a function of temperature. The marked change in response above and below the T_g necessitated the use of a logarithmic y-axis for clarity. The step change in properties can be seen between the 21 and 40˚C curves. At temperatures between -20 and 21˚C a post yield drop can be observed reminiscent of a smeared out version of the yield drop seen in many steels. It will be seen that samples below T_g were less elastic upon unloading having a larger residual strain.

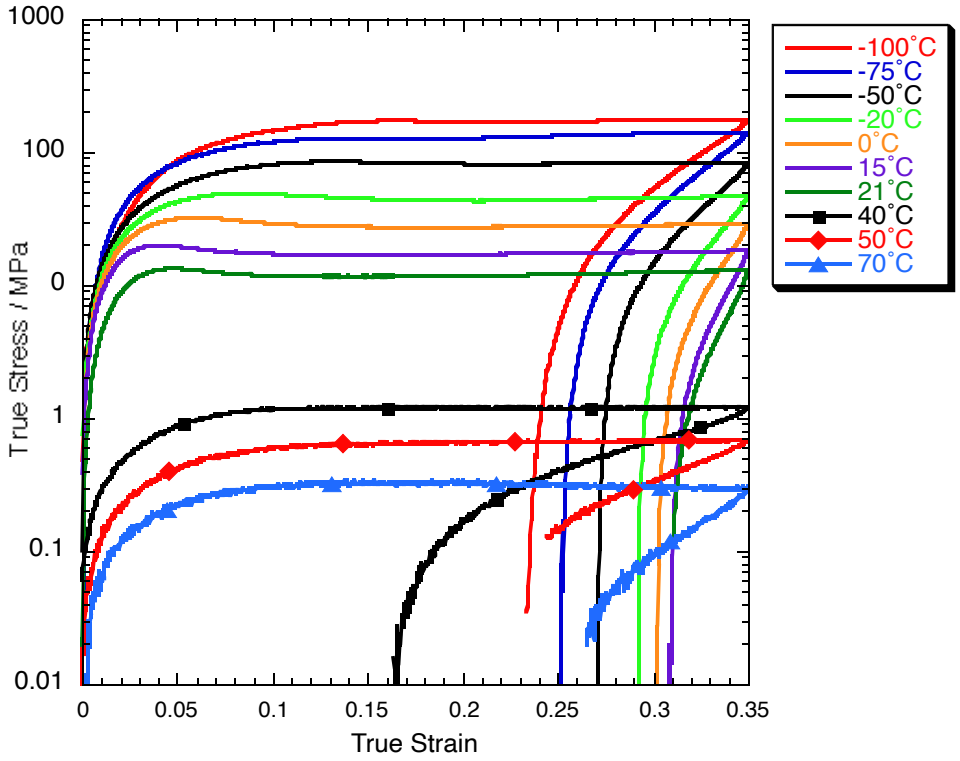

Figure 3. The compressive response of the 5% billet as a function of temperature (1×10^{-3} s^{-1})

The effect of strain-rate on the compressive response is shown in figure 4. In tests up to 1 s^{-1}, the crosshead can be reversed and the unloading curve resolved. This is not possible at higher rates. The origins of the post yield oscillations at 5, 10 and 15 s^{-1} are not known but are thought to be real material effects because similar oscillations have not been observed in many other polymers tested in an identical fashion. Because the tests were undertaken at room temperature a clear post yield drop is evident in all curves above 1×10^{-4} s^{-1}.

The loading modulus (some might say Young's modulus) increases as a function of strain-rate and a plot of this value and the value as function of temperature is displayed in figure 5. It will be seen that on single axis logarithmic plots both the strain-rate and temperature trends follow a linear pattern, however there is a break in the temperature gradient at T_g.

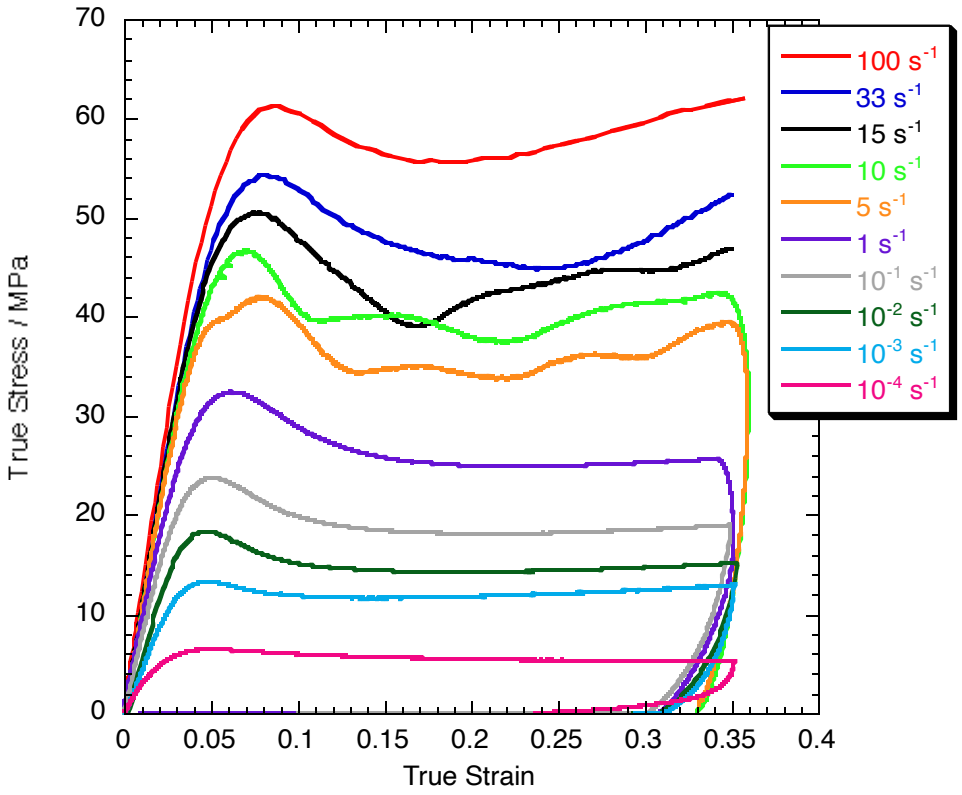

Figure 4. The compressive response of the 5% billet as a function of strain-rate (21˚C).

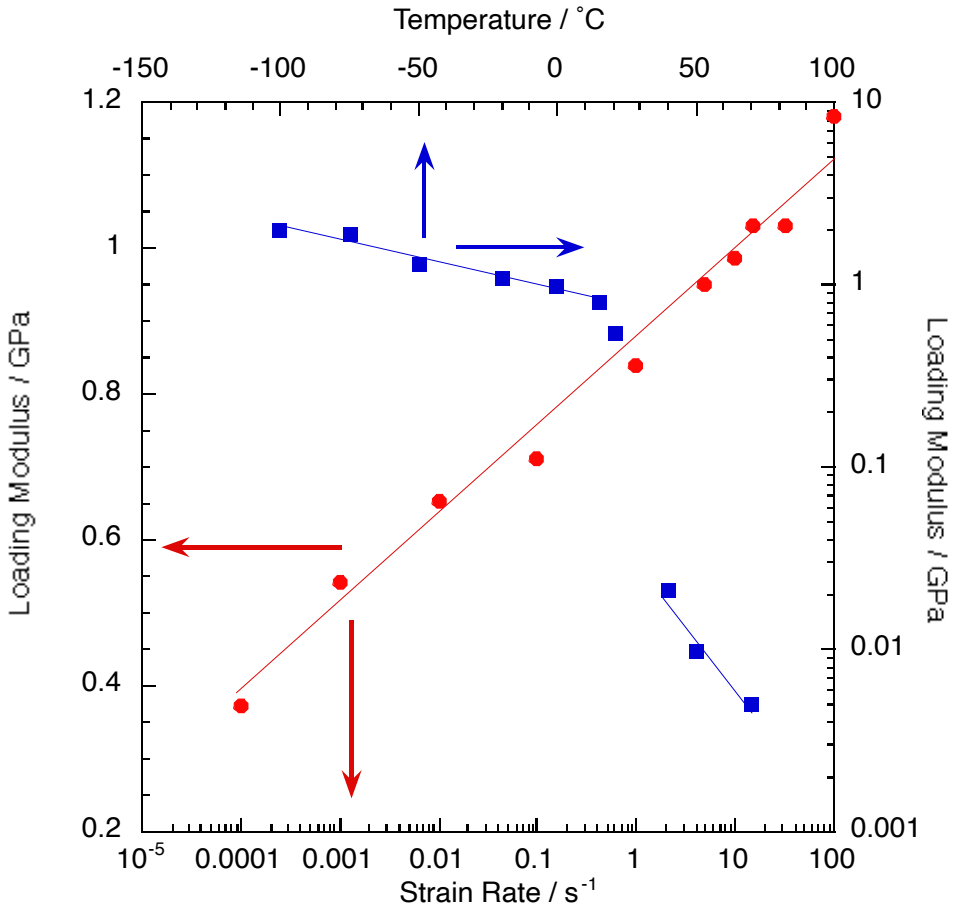

Figure 5. The loading modulus as a function of temperature and strain-rate. The colored linear lines indicate trends rather than being analytic lines of best fit.

The compressive response at higher strain-rate is shown in figure 6 as a function of temperature. As before, a change in flow stress occurs above T_g, however at this strain-rate the change in magnitude is significantly reduced. In all cases strain softening is observed. The maximum flow stress occurs at approximately 0.1, this is higher than the compressive data shown in figure 4, however, extrapolation to the higher strain-rate shows this to be reasonable.

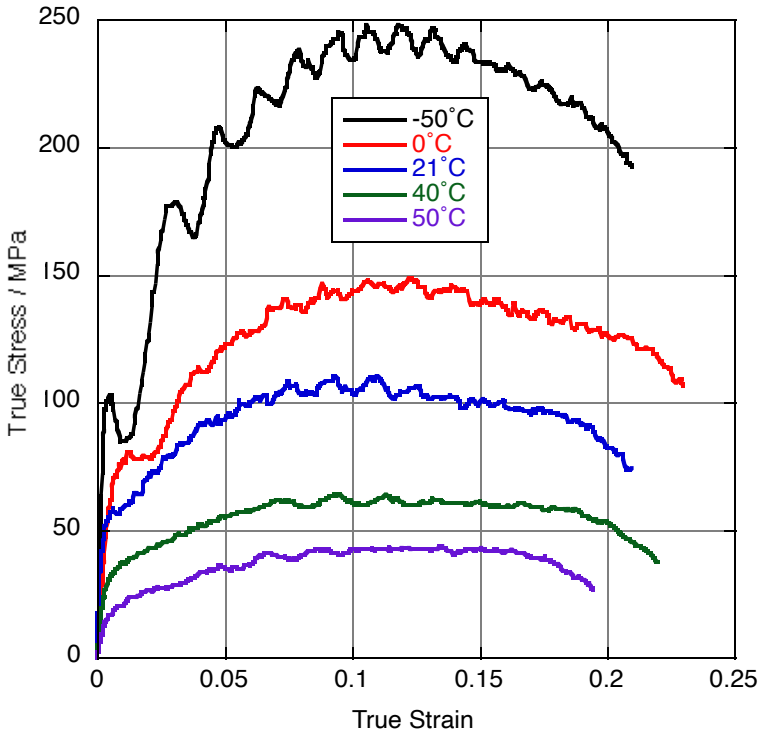

Figure 6. Compressive Hopkinson bar stress vs. strain data as a function of temperature. Strain-rate 3200±200 s^{-1}.

The compressive yield stress as a function of strain-rate can be extracted and plotted (figure 7). As found in other polymers [9, 10], an empirical power law may be adequately fit to the data. The reason for this is not known.

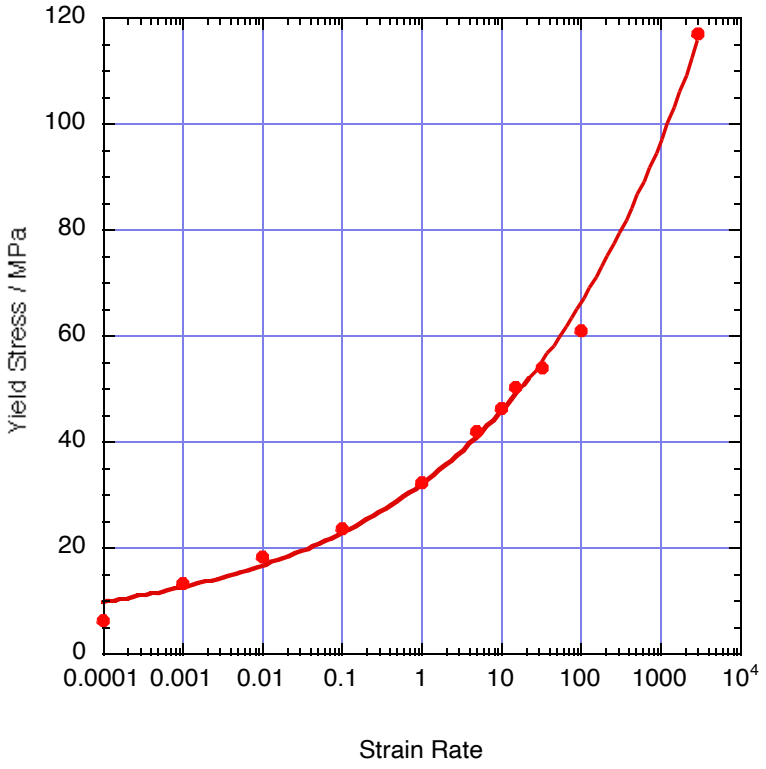

Figure 7. The compressive yield stress plotted as a function of strain-rate. The line of best fit is to an empirical power law, $y=a+bx^c$, where a=4.115, b=27.81 and c=0.1734.

The tensile response of 5% Kel-F 800 as a function of temperature is shown in figure 8. At temperatures below T_g, failure was induced in all samples, however above T_g failure could not be induced before the maximum observable strain of 700% (engineering). Below T_g, a marked post yield drop in stress is observed prior to strain hardening, however above T_g this does not occur. As expected, the strain to failure decreases with decreasing temperature.

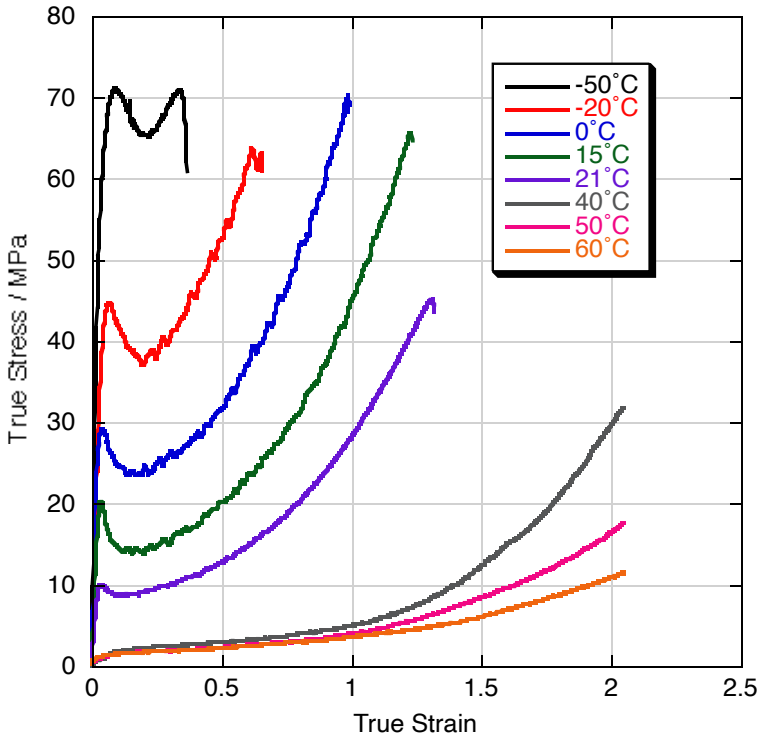

Figure 8. The tensile response as a function of temperature (5×10^{-3} s^{-1}). Samples at 40-60˚C did not fail at the maximum observable strain of 700% (engineering).

The effect of strain-rate on the tensile response is shown if figure 9. The yield strength increases with increasing rate and the strain to failure was lower at the two highest rates tested. The post yield drop is more significant at higher strain-rates. The range of strain-rates at which the video extensometer can be used is more limited in tension than in compression accounting for the fewer curves.

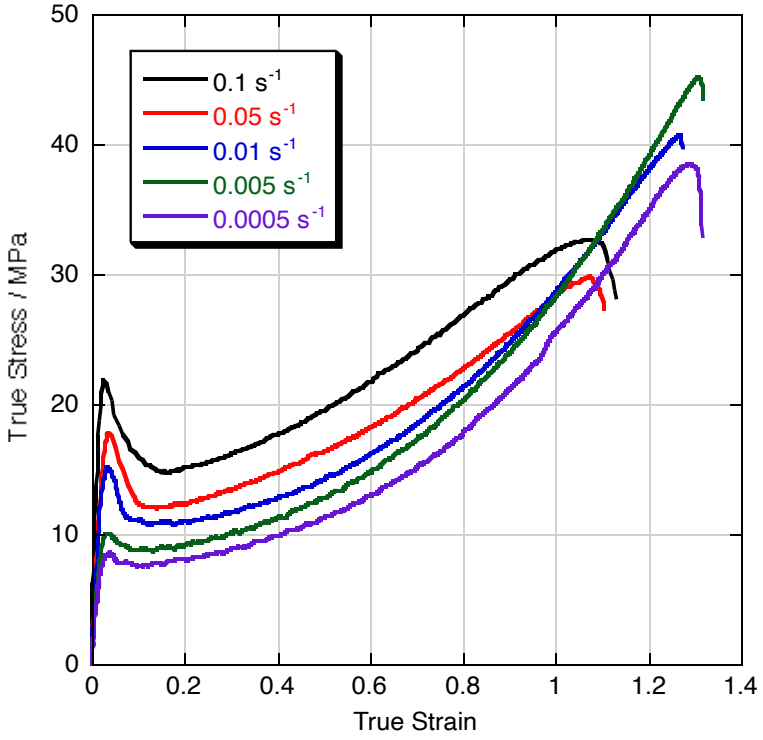

Figure 9. The tensile response as a function of strain-rate (21±1˚C). Failure was induced in all samples.

Annealing Study Results

Amorphous Material

Granules from lot 30013 were placed in rectangular PTFE moulds and heated in a vacuum oven to 130˚C. Over approximately 48 hours, the material was cycled between ambient air pressure and vacuum until all visible gas bubbles were removed from the melt. The moulds were then removed from the oven and quickly cooled in a forced room air draft. In this way, small 100×50x10 mm^3 essentially amorphous billets were produced. Samples for tension and compression analysis were machined as well as rough sawn bars for crystallization studies.

The compressive response at five temperatures is shown in figure10. The material has almost no strength above T_g in the amorphous state. In contrast, the flow stress at −50˚C is essentially identical to the 5% reference billet.

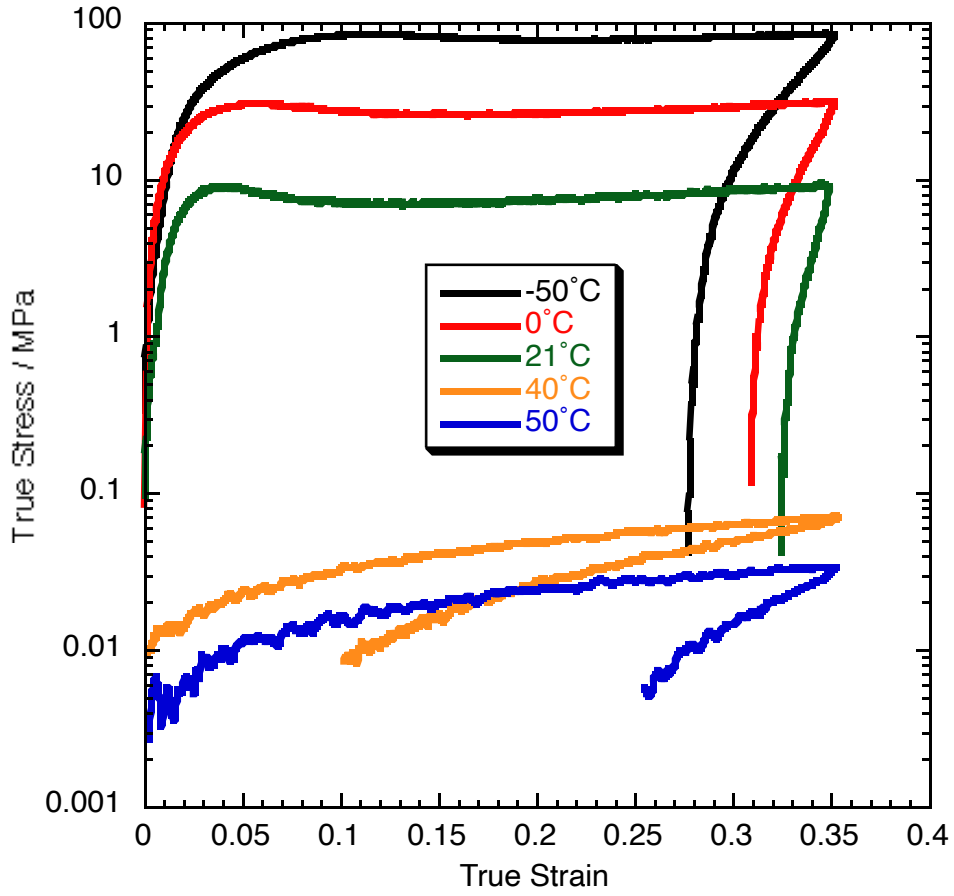

Figure 10. Compressive stress/strain response of amorphous Kel–F 800 at 1×10^{-3} s^{-1}.

The room temperature compressive response as a function of strain-rate is shown in figure 11. It will be noticed that the material did not significantly relax upon unloading indicating significant permanent plastic strain in the sample. As in the 5% crystallinity billet, a significant post-yield drop is observed at strain-rates above 1×10^{-4} s^{-1}.

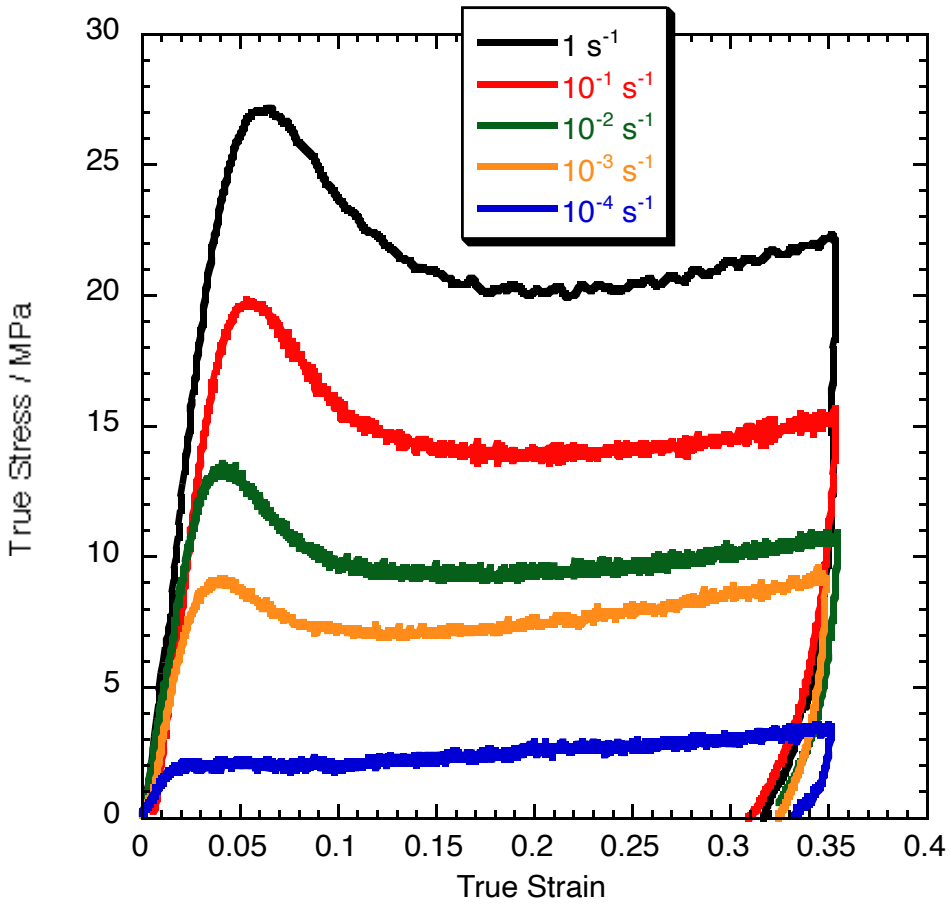

Figure 11. Compressive stress/strain response of amorphous Kel–F 800 as a function of strain-rate (21˚C).

The tensile response at four temperatures is shown in figure 12. The strain to failure at 21˚C is very similar to the 5% billet, however, the failure stress is about a quarter of that in the higher crystallinity material. Above T_g, the material had almost no strength until a true strain of about 1.5. At this point, a localization formed and the material failed within the extensometers field of view.

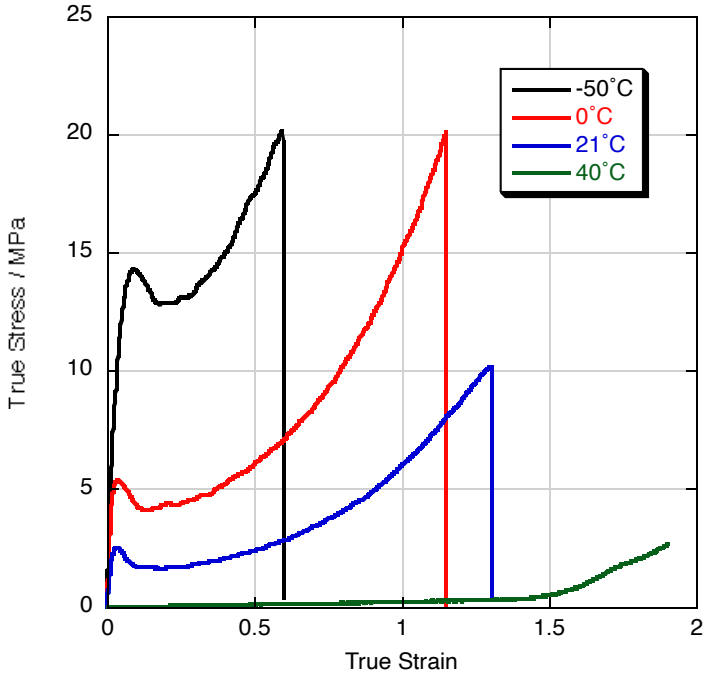

Figure 12. Tensile stress/strain response of amorphous Kel–F 800 at 1×10^{-3} s^{-1}.

The tensile response as a function of strain-rate is shown in figure 13. The data are unremarkable except for the lower stresses generated for a given strain with respect to the 5% reference billet.

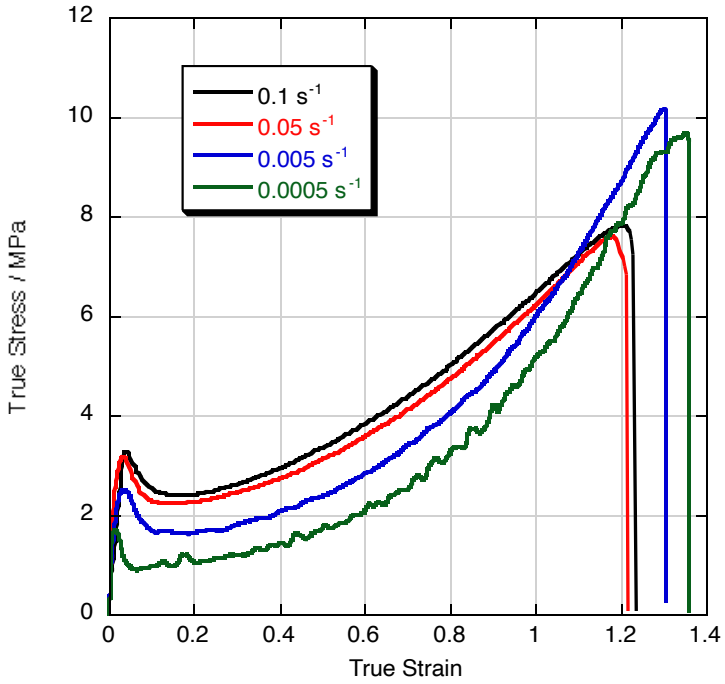

Figure 13. Tensile stress/strain response of amorphous Kel–F 800 as a function of strain-rate (21˚C).

The DMA response was measured for the amorphous and 5% billet material at four frequencies. In figure 14 the response for the amorphous material is shown. The scan had to be stopped at 50˚C because the material became too soft for the machine to test. Figure 15 shows the response of 5% material for comparison. Below T_g there is little observable difference in response. Above T_g the scan could be continued to 100˚C for the 5% crystallinity material with the higher frequency data being valid to 70˚C. At higher crystallinity the 'elastic' (G') modulus plateaus a little below 10^8 dynes cm^{-2} (10 MPa) and remain there until melt. In the case of the amorphous material, the G' modulus continues dropping to 10^7 dynes cm^{-2} (1 MPa) before the scan ends.

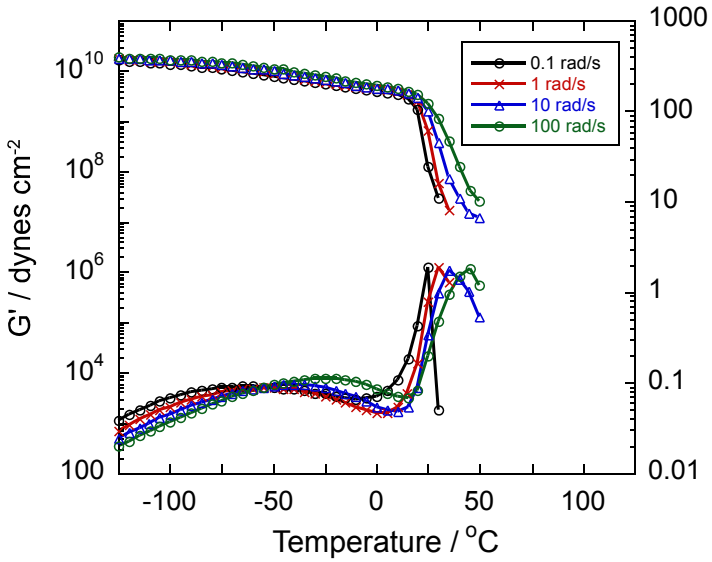

Figure 14. DMA results for amorphous Kel-F 800.

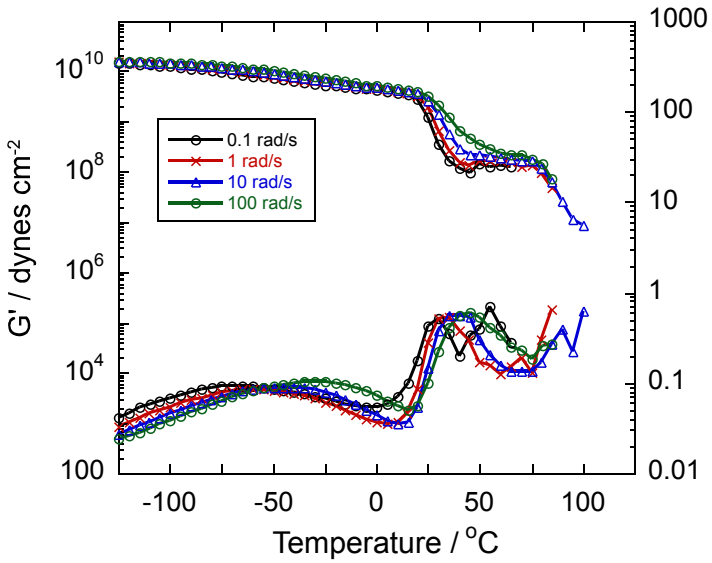

Figure 15. DMA results for the reference 5% billet.

100 Days at 40˚C

To simulate the properties of stockpile returned Kel-F 800 within PBX 9502 a billet of approximately 5% starting crystallinity was annealed for 100 days at 40˚C. After this time previous crystallinity studies suggest near maximum crystallinity should have achieved for this temperature. The properties in compression and tension were measured for comparison with the 5% billet. The measured crystallinity from DSC was 12.4% after this annealing process.

The compressive properties as a function of temperature are shown in figure 16. As before the change in properties above and below T_g is obvious. At -50˚C the flow stress response is very similar to the reference 5% billet but above T_g, the flow stress is significantly enhanced by the extra crystallinity. The samples above T_g showed significant strain softening that was not seen in either the amorphous or 5% crystalline material at similar temperatures.

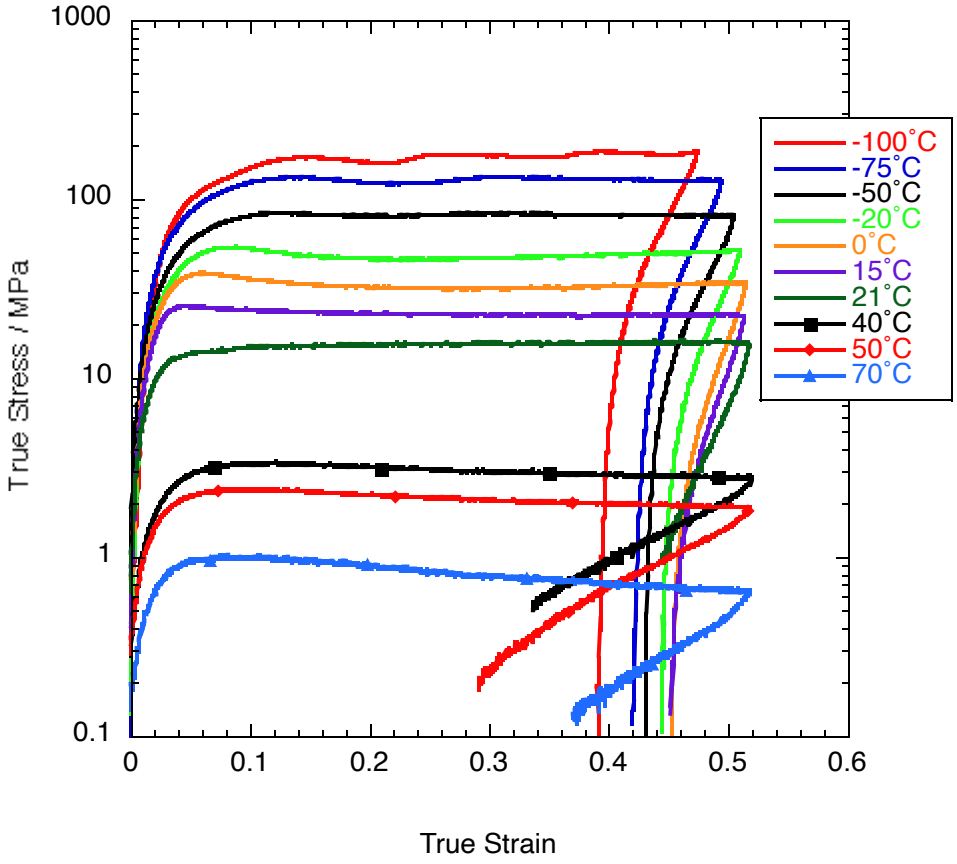

Figure 16. The compressive stress response as a function of temperature for material aged for 100 days at 40˚C (1×10^{-3} s^{-1}).

The compressive response as a function of strain-rate is shown in figure 17. The flow stress is higher in all cases than the 5% reference material but the large strain response is different. In the 5% reference material, above 20% strain all the curves except 10^{-4} s^{-1} showed strain hardening. On the contrary, in this highly annealed material, the

10^{-4} s^{-1} and 10^{-3} s^{-1} curves show strain hardening while the faster tests show a softening behavior.

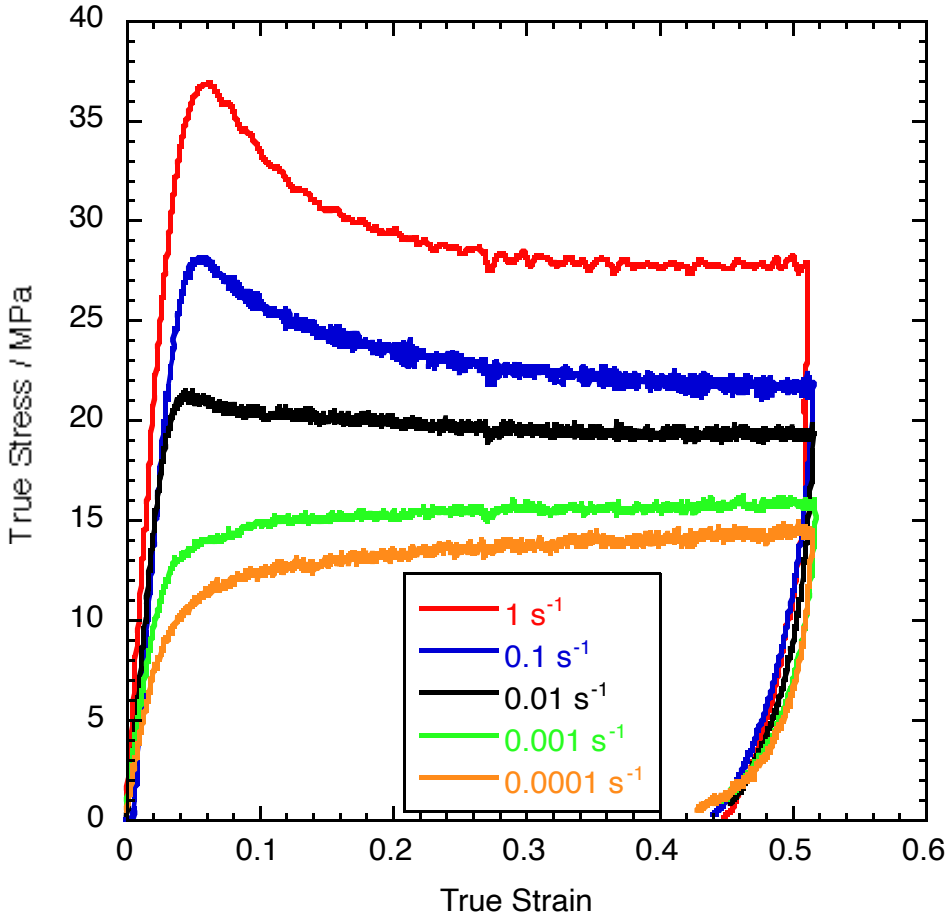

Figure 17. The compressive stress response as a function of strain-rate for material aged for 100 days at 40˚C (test temperature 21˚C).

The tensile response as a function of temperature is shown in Figure 18. The inset graph shows the large strain response at 40 and 50˚C. The increased crystallinity had a marked effect on the tensile response over the reference billet. In all cases below T_g the strain to failure was reduced, sometimes greatly. Additionally, at 23˚C and higher a localized neck formed that began to draw out. In the case of 23 and 50˚C, this neck region failed in the extensometers field of view, however, at 40˚C the neck had not failed before maximum observable strain. At 0, -20 and -50˚C the strain to failure was so low that instead of the video extensometer, a traditional clip-on extensometer was used. At these temperatures, no localization was noted before brittle failure of the sample.

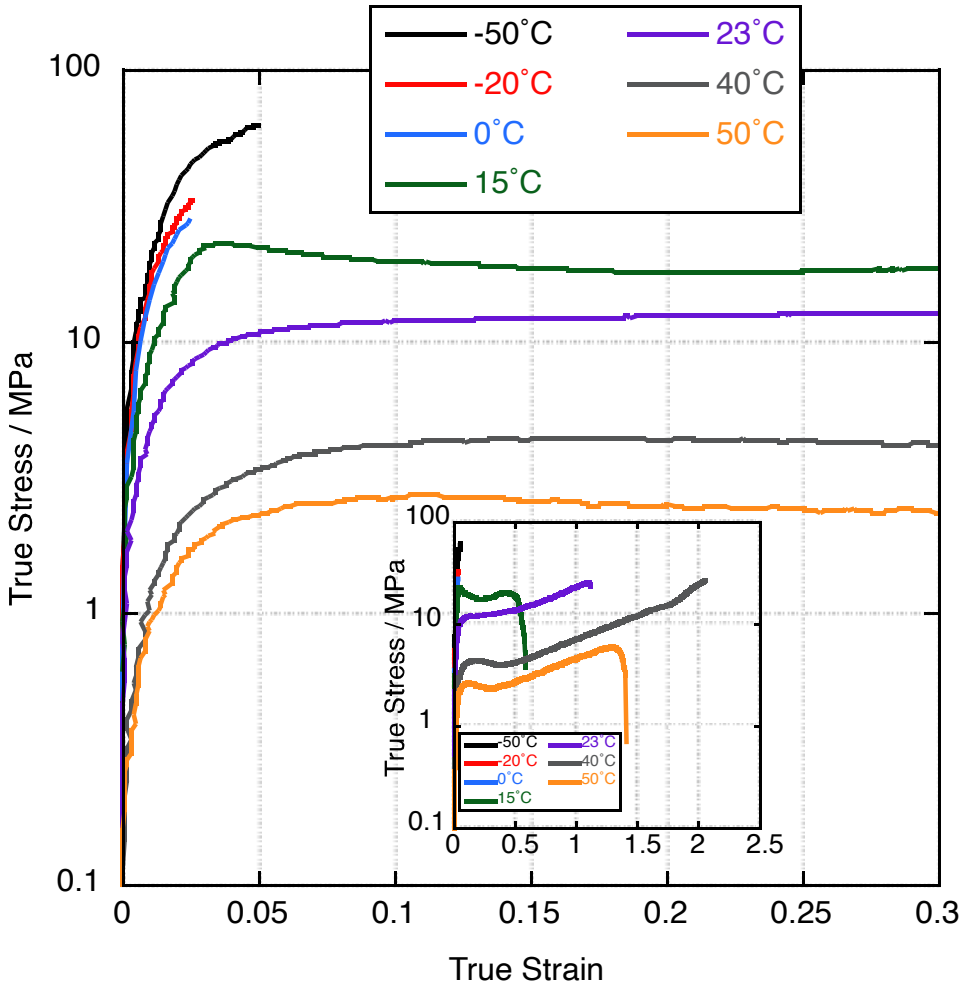

Figure 18. The tensile stress response as a function of temperature for material aged for 100 days at 40˚C (1×10^{-3} s^{-1}).

The tensile response at three strain-rates is shown in figure 19. Possibly because of the formation of the localization in this high crystallinity material, no yield drop is observed, but the strain to failure is much reduced at the higher rates.

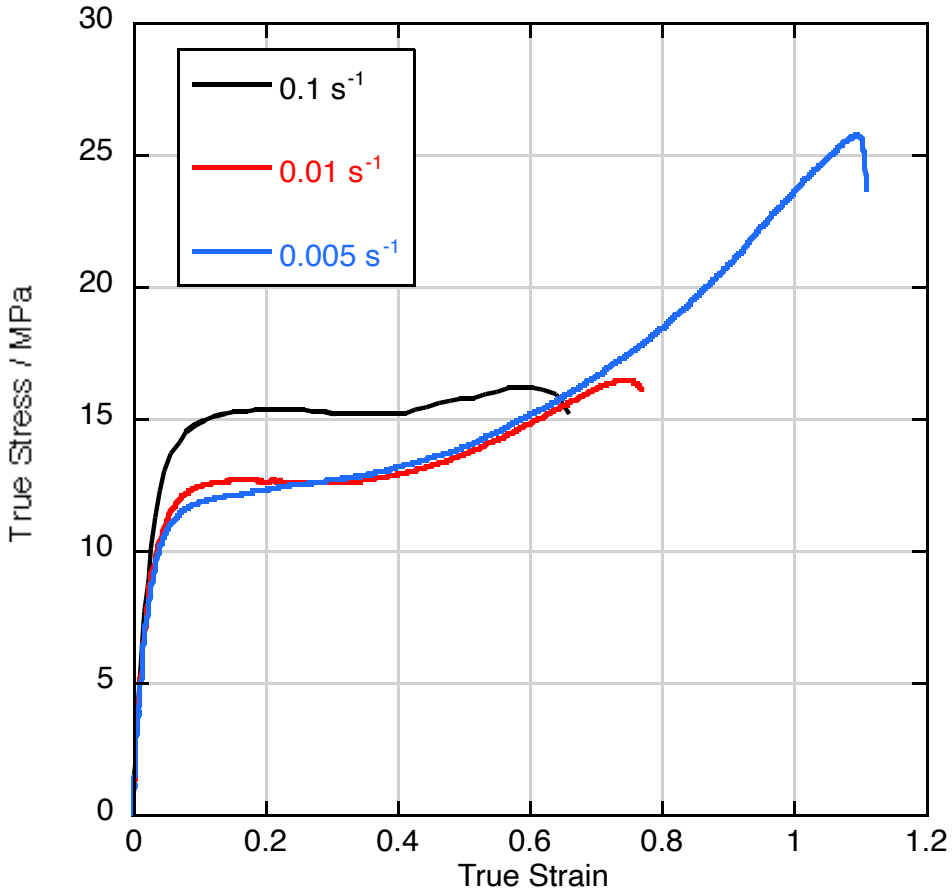

Figure 19. The tensile stress response as a function of strain-rate for material aged for 100 days at 40˚C (21˚C).

65˚C annealing study from 5% billet start.

Bar samples were rough saw from the 5% billet for an annealing study at 65˚C that lasted 82 days. Samples were removed from the oven at intervals and subjected to DSC analysis and compression at two temperatures. Figure 20 shows the DSC results, for T_g, melt temperature and melt endotherm. The T_g remains unchanged by the annealing process while the melt temperature increases with time towards an asymptotic value. The crystallinity (melt endotherm) increases exponentially towards a maximum value that is reached early into the study at this particular temperature and starting crystallinity.

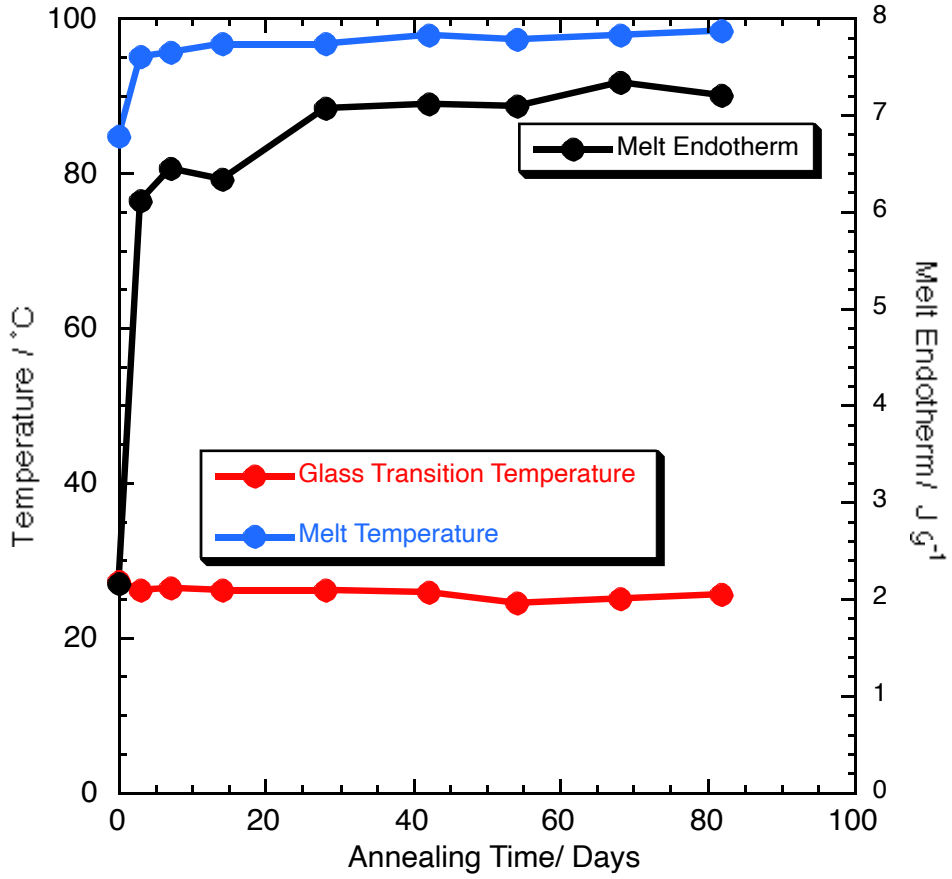

Figure 20. Results from DSC analysis of samples removed from an annealing study at 65˚C. The starting material was from the 5% billet.

Figures 21 and 22 show the compressive response at 21 and 70˚C respectively (at strain-rate of 1×10^{-3} s^{-1}). It will be seen that there is a marked increase in strength in both cases between the starting crystallinity and the 3-day material. Towards the end of the study, little change in properties is observed. This is in agreement with the DSC results. As expected, the increased crystallinity has a significant effect above T_g when the crystalline regions will inhibit amorphous region deformation. It is also clear that above T_g, increased crystallinity produces a more rubbery material (i.e. the material returns back closer to its starting dimensions upon unloading). Significantly, the post-yield drop disappears at 21˚C after only 3 days at the annealing temperature. As the crystallinity increases with time, only monotonic strain hardening is seen. In all cases at 70˚C, strain softening is seen but the gradient is steeper at higher crystallinities.

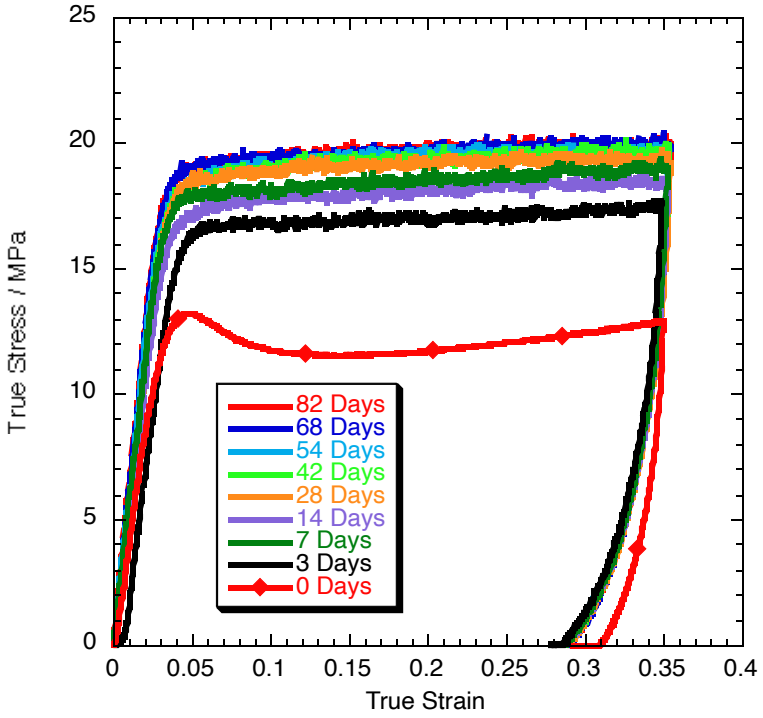

Figure 21. Stress vs. strain response at 21˚C from the annealing study at 65˚C (1×10^{-3} s^{-1}).

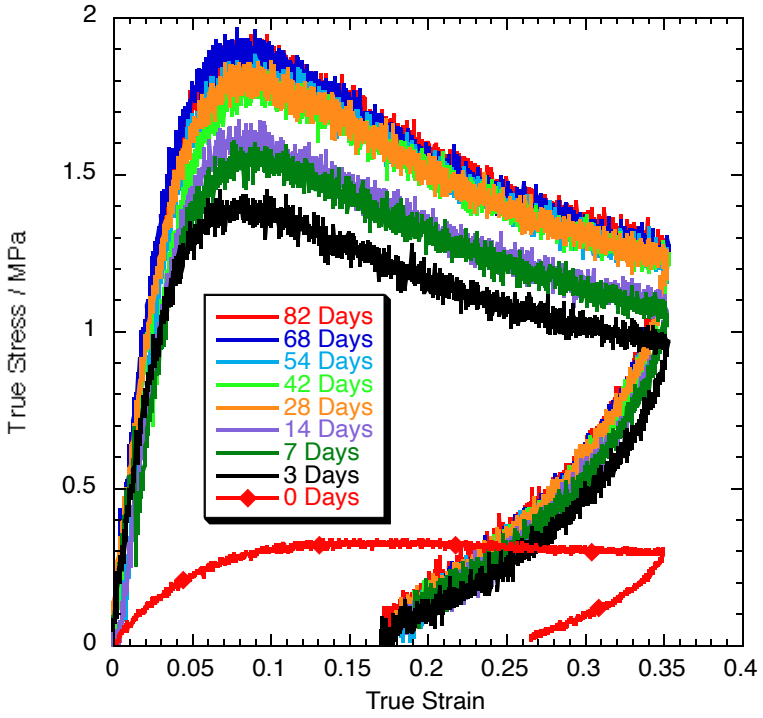

Figure 22. Stress vs. strain response at 70˚C from the annealing study at 65˚C (1×10^{-3} s^{-1}).

The yield stress at both temperatures is compared in figure 23. Extra crystallinity quickly increases the strength at 70˚C when the material is well above the glass transition temperature although it remains approximately a factor of 10 lower than at 21˚C.

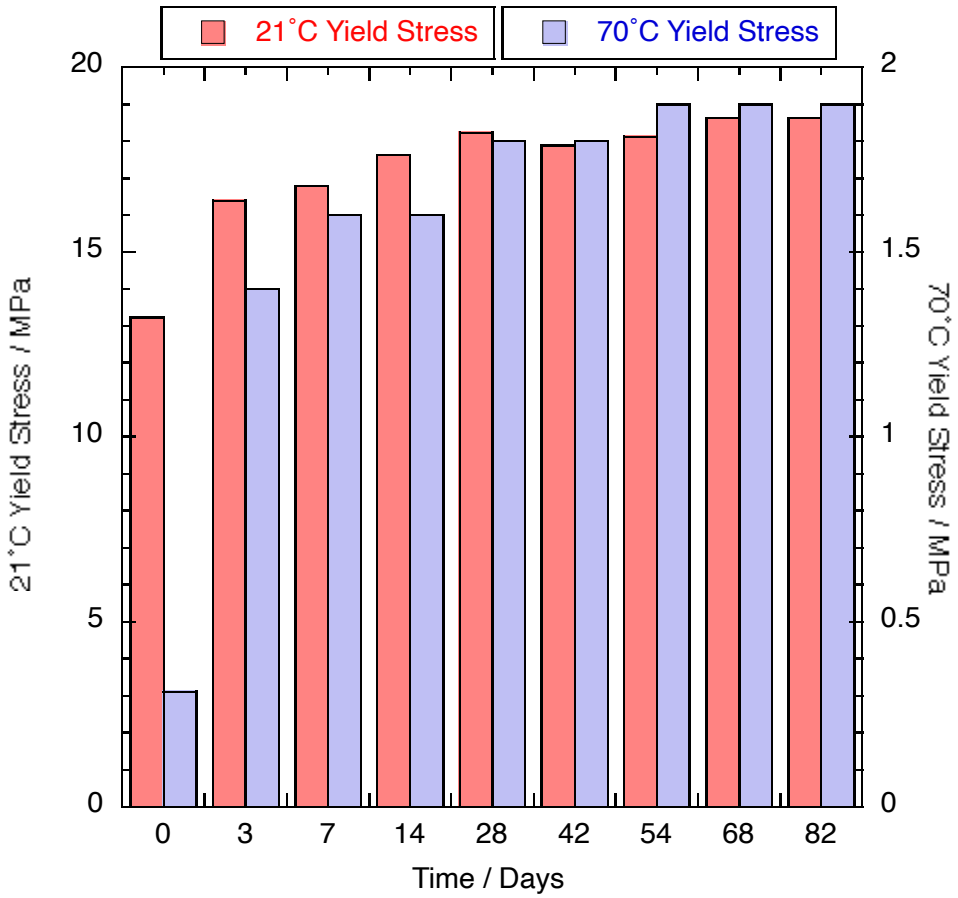

Figure 23. Yield stress vs. annealing time for the 65˚C study.

40˚C Crystallization study from an amorphous start.

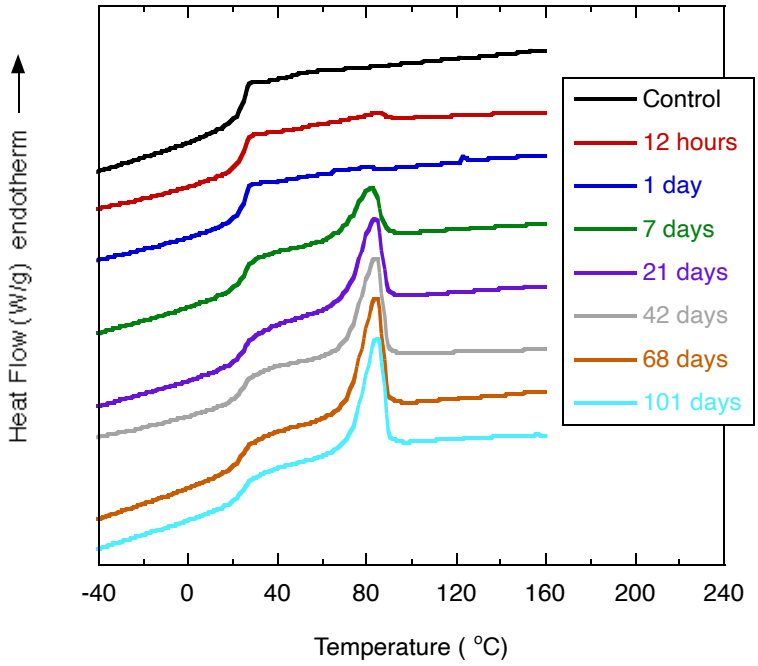

Figure 24. DSC Curves for amorphous material annealed at 40˚C.

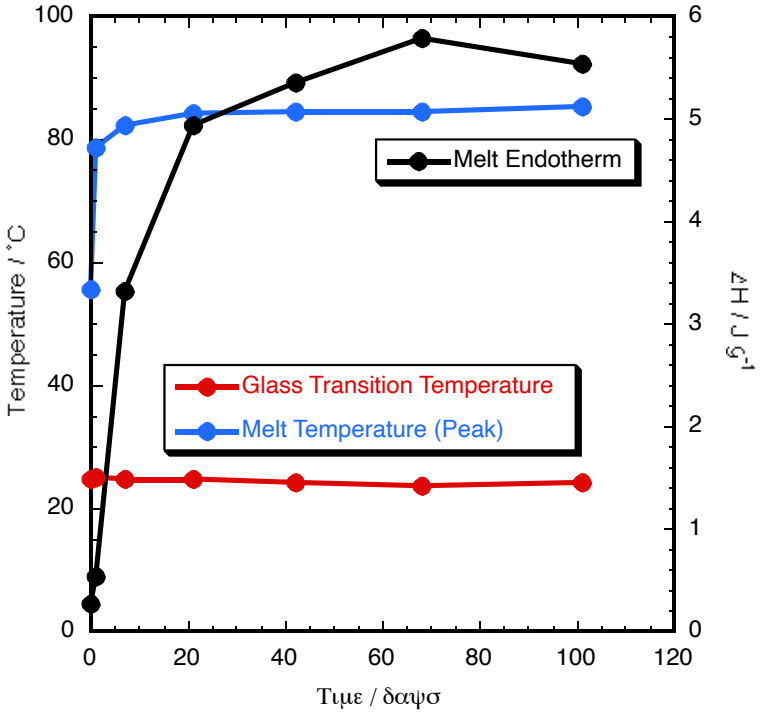

Figure 25. Summary of T_g, Tm and melt endotherm for amorphous material annealed at 40˚C

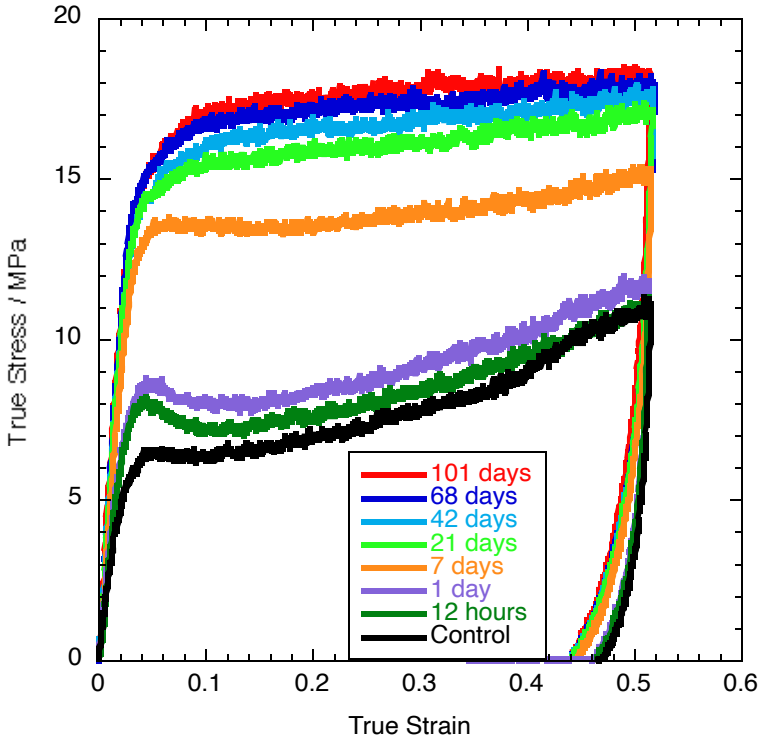

Figure 26. Compression response at 21˚C of amorphous material annealed at 40˚C

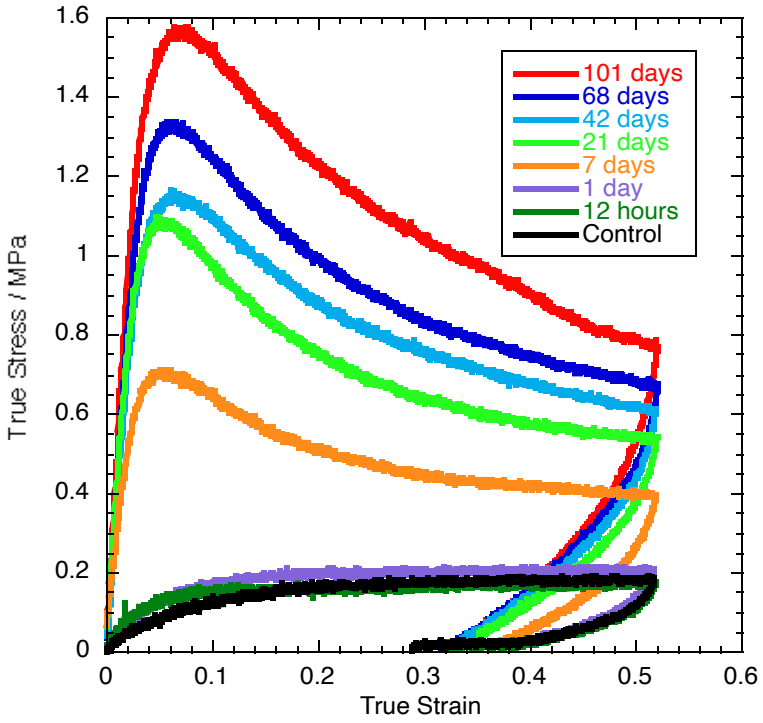

Figure 28. Compression response at 70˚C of amorphous material annealed at 40˚C

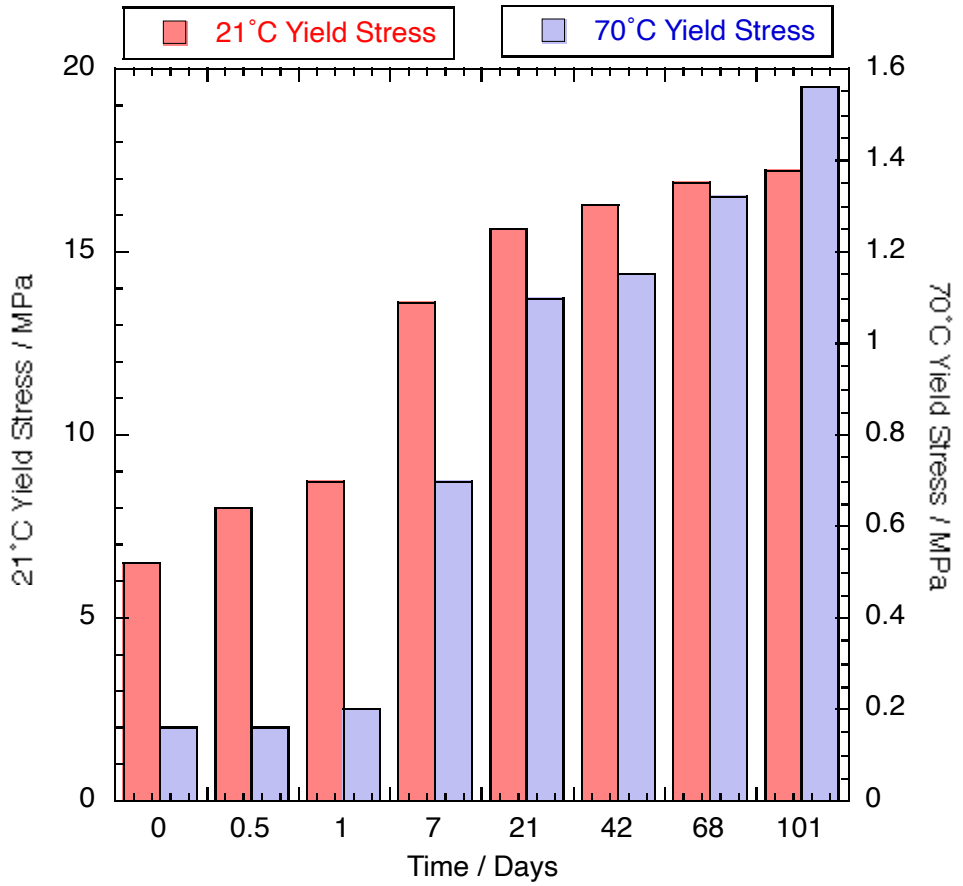

Figure 29. Summary graph of yield stress vs. annealing time for amorphous material annealed at 40˚C.

50˚C Crystallization study from an amorphous start.

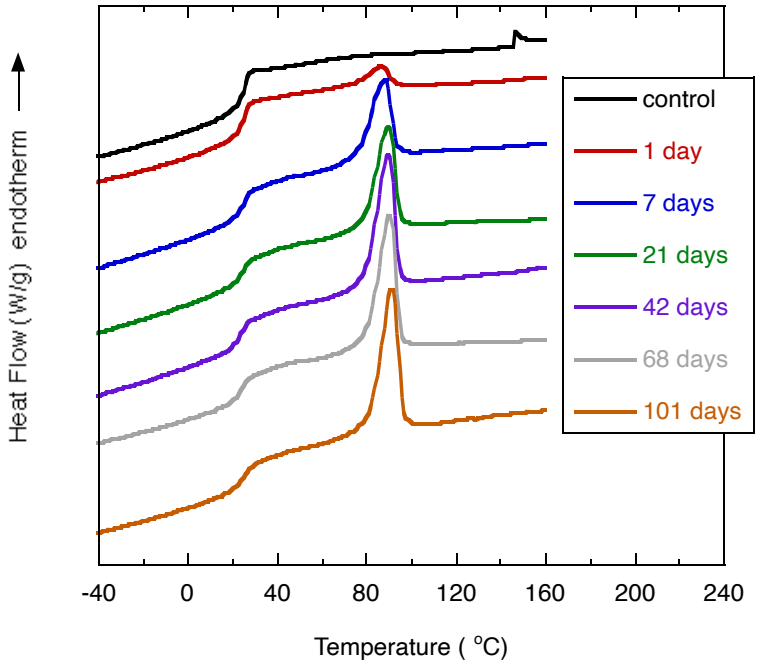

Figure 30. DSC Curves for amorphous material annealed at 50˚C.

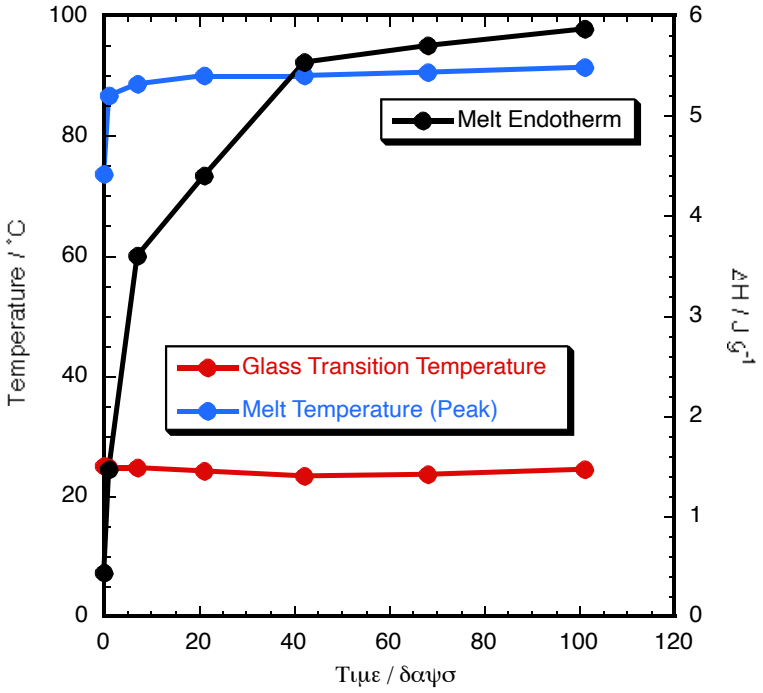

Figure 31. Summary of T_g, Tm and melt endotherm for amorphous material annealed at 50˚C.

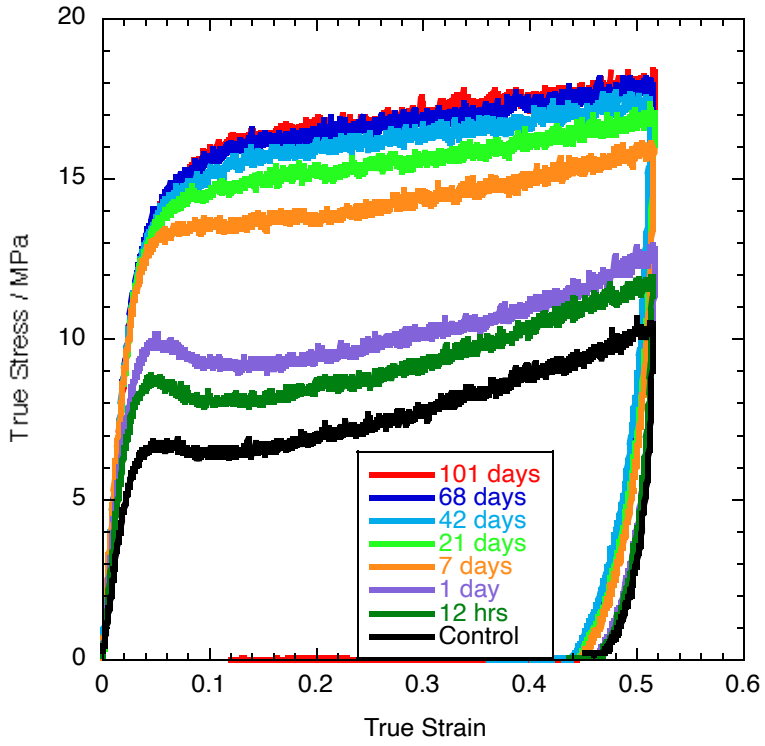

Figure 32. Compression response at 21˚C of amorphous material annealed at 50˚C

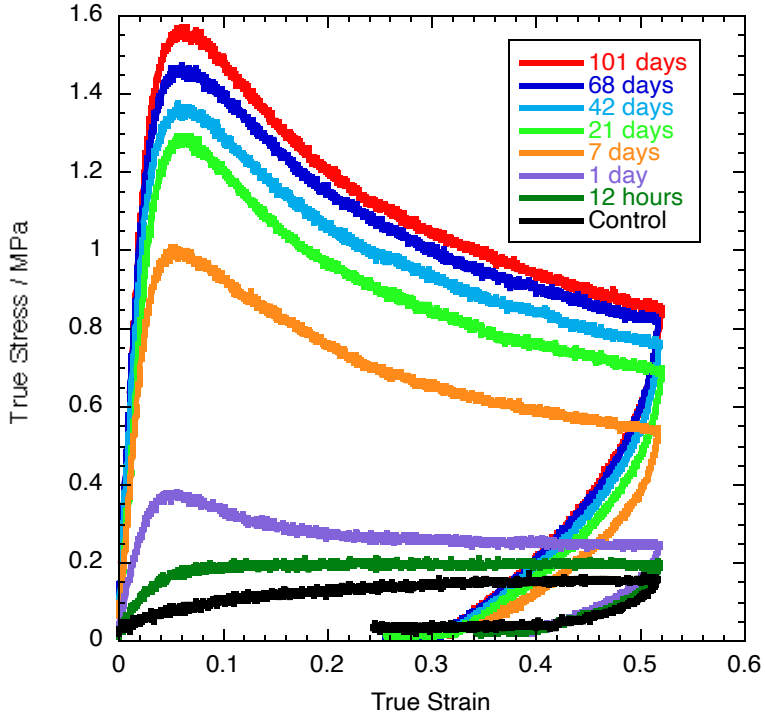

Figure 33. Compression response at 70˚C of amorphous material annealed at 50˚C

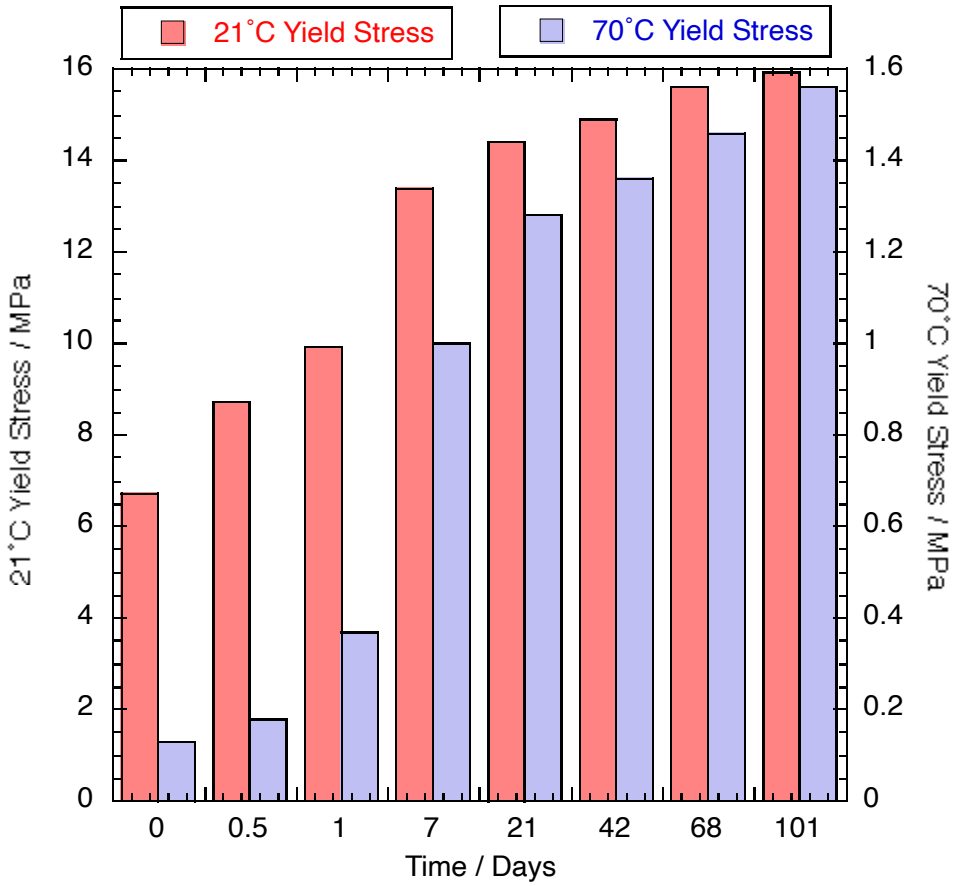

Figure 34. Summary graph of yield stress vs. annealing time for amorphous material annealed at 50˚C.

30˚C Crystallization study from a low crystallinity billet.

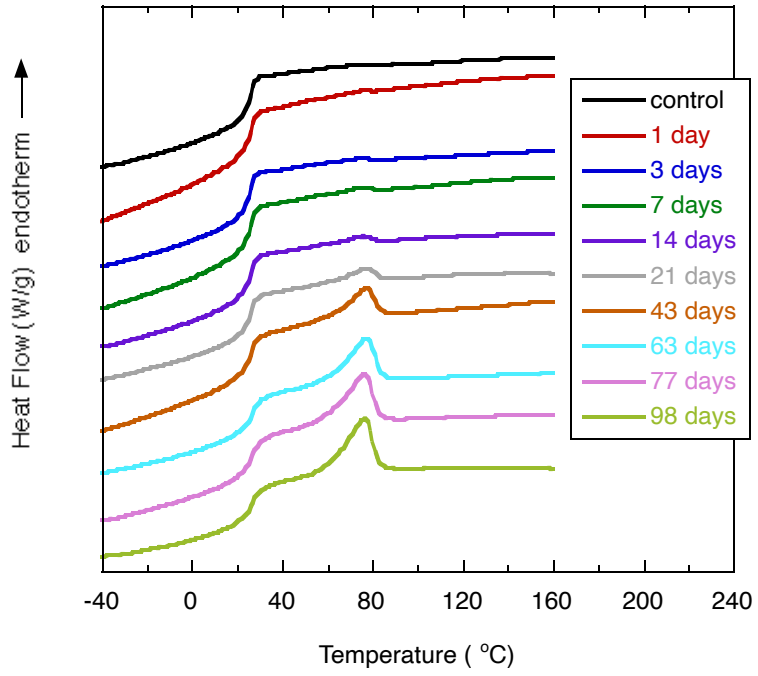

Figure 35. DSC Curves for billet start material annealed at 30˚C.

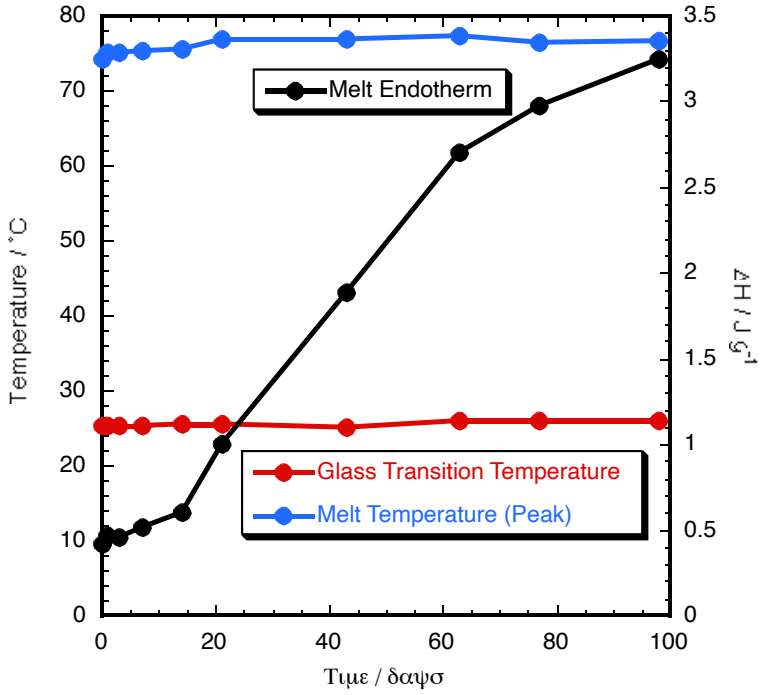

Figure 36. Summary of T_g, Tm and melt endotherm for billet material annealed at 30˚C.

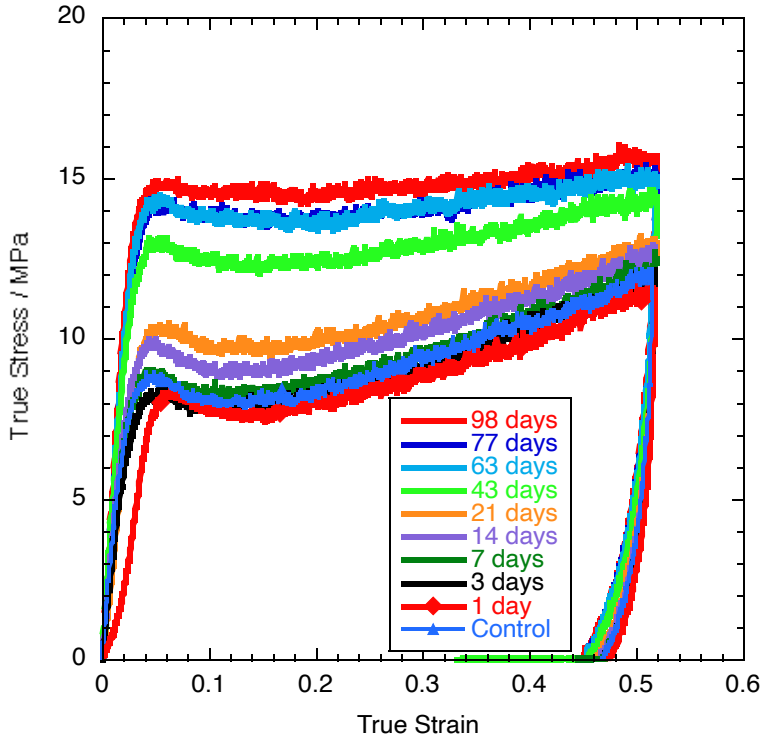

Figure 37. Compression response at 21˚C of billet material annealed at 30˚C.

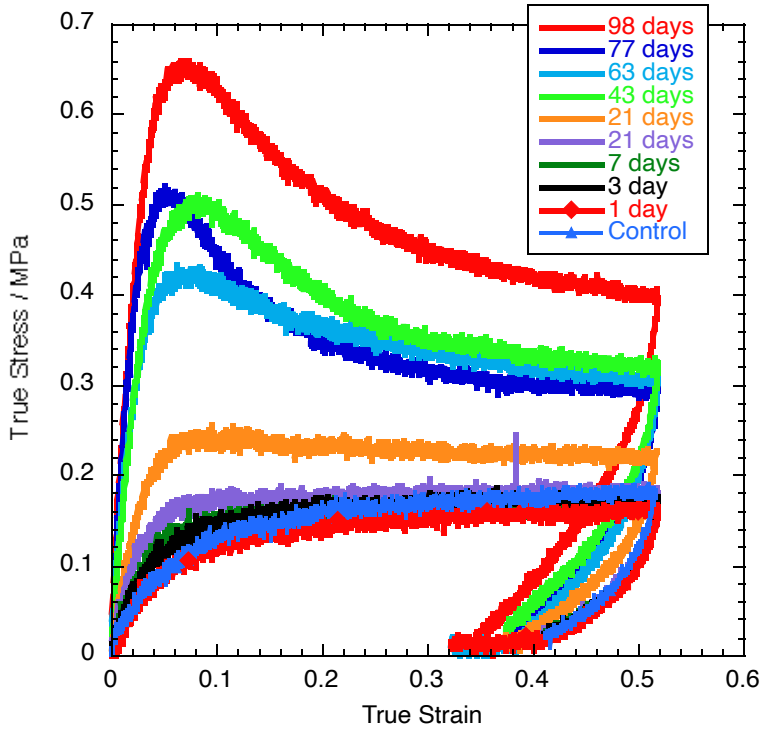

Figure 38. Compression response at 70˚C of billet material annealed at 30˚C.

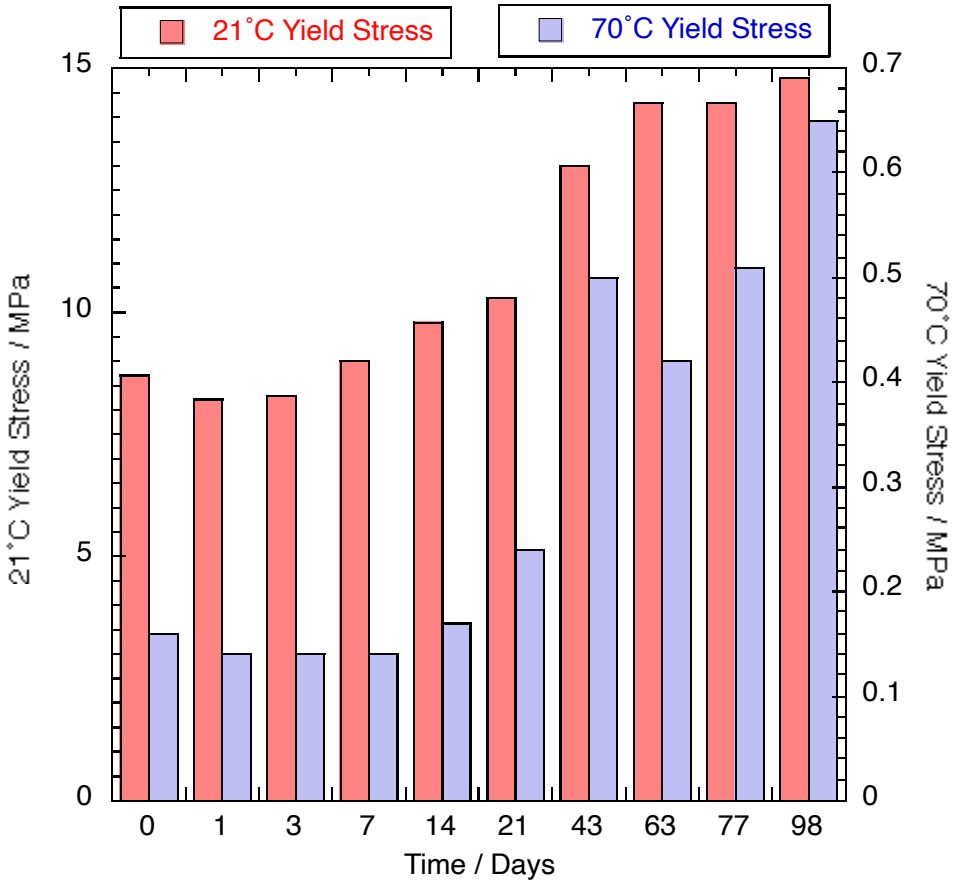

Figure 39. Summary graph of yield stress vs. annealing time for billet material annealed at 30˚C.

35˚C Crystallization study from a low crystallinity billet.

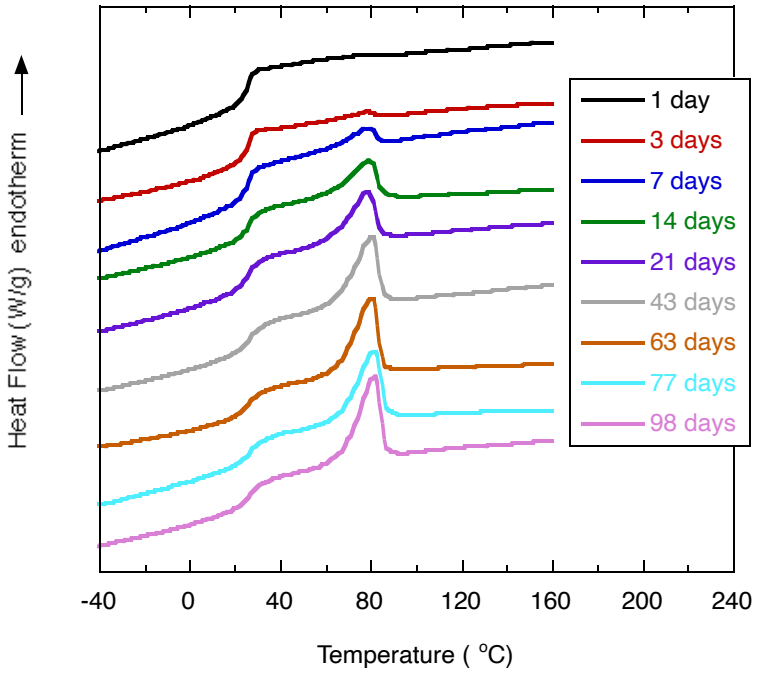

Figure 40. DSC Curves for billet start material annealed at 35˚C.

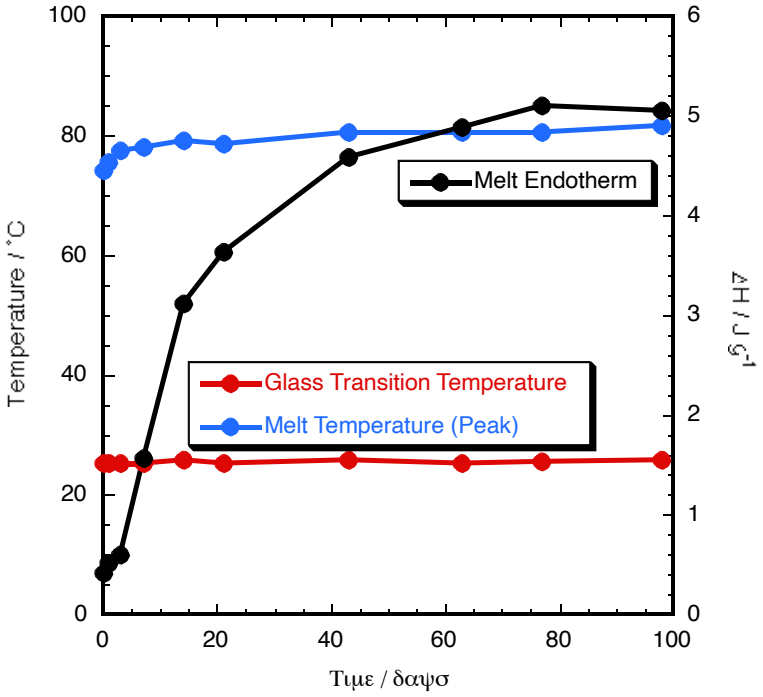

Figure 41. Summary of T_g, Tm and melt endotherm for billet material annealed at 35˚C.

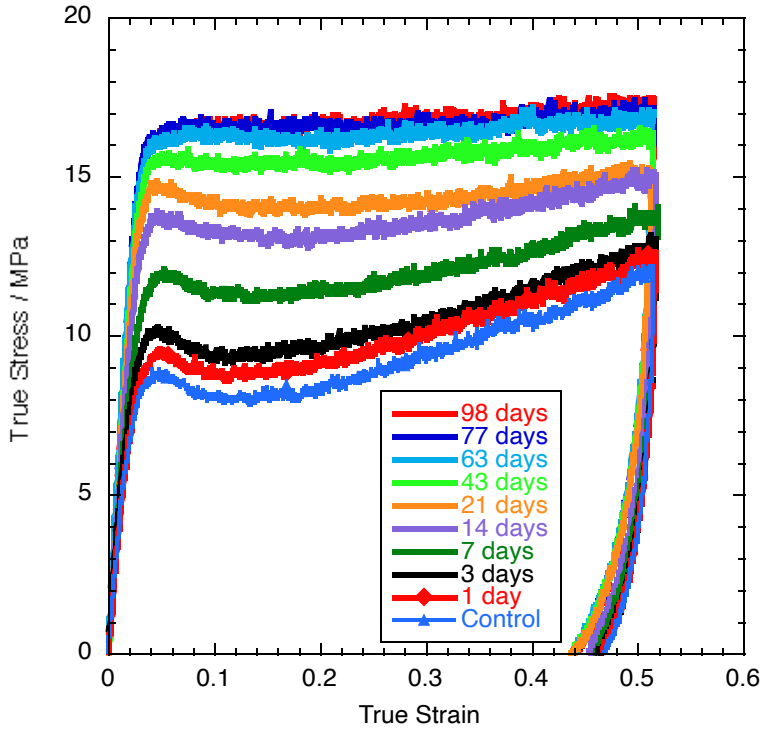

Figure 42. Compression response at 21˚C of billet material annealed at 35˚C.

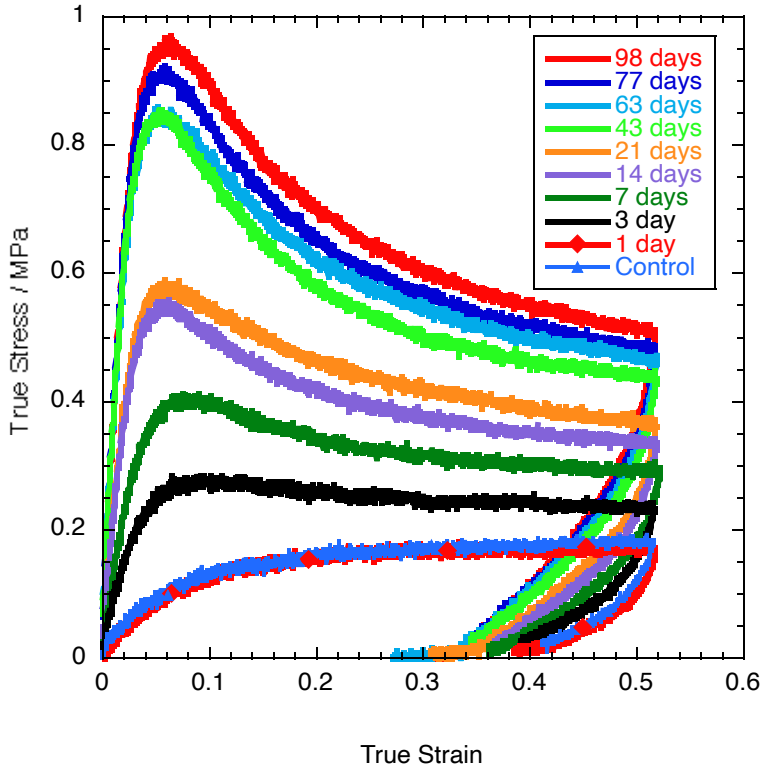

Figure 43. Compression response at 70˚C of billet material annealed at 35˚C.

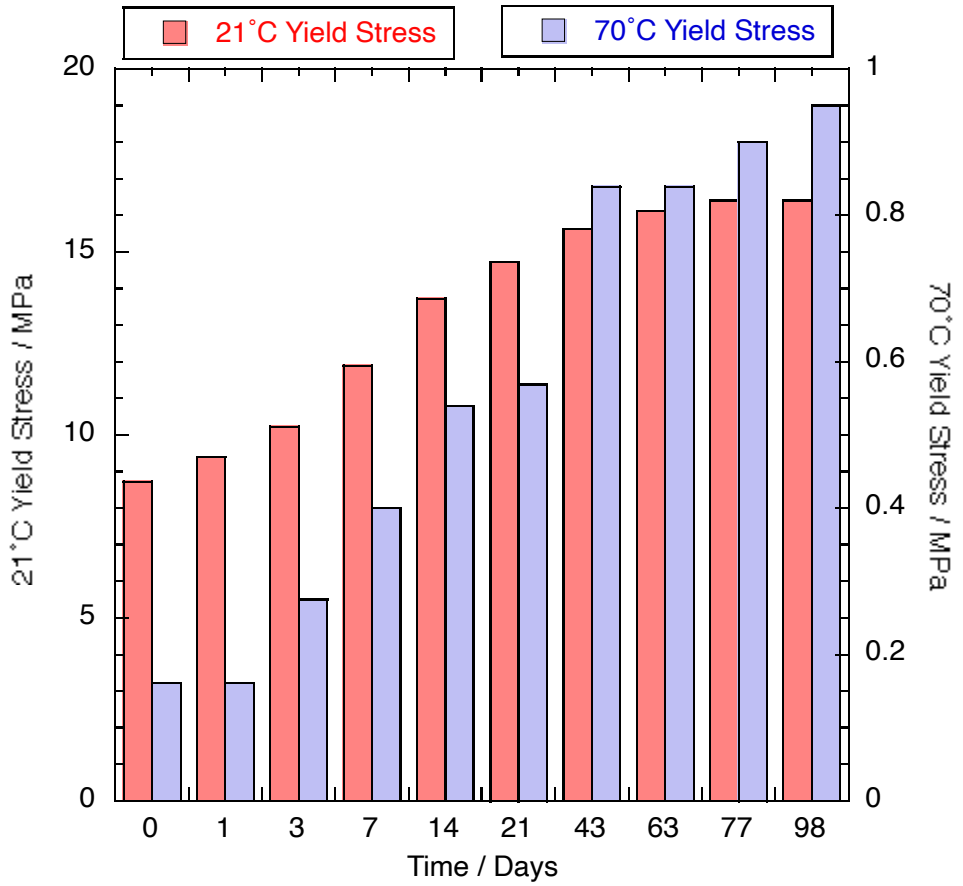

Figure 44. Summary graph of yield stress vs. annealing time for billet material annealed at 35˚C.

40˚C Crystallization study from a low crystallinity billet.

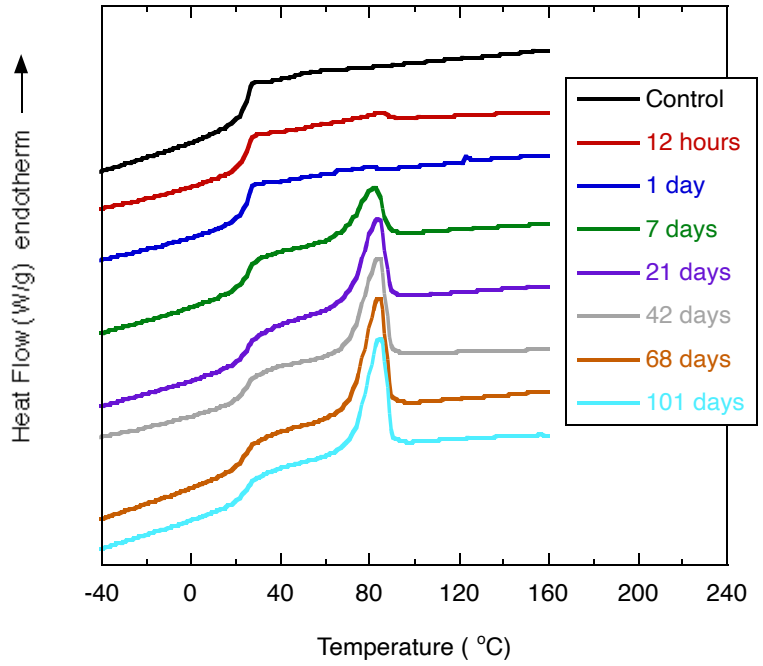

Figure 45. DSC Curves for billet start material annealed at 40˚C.

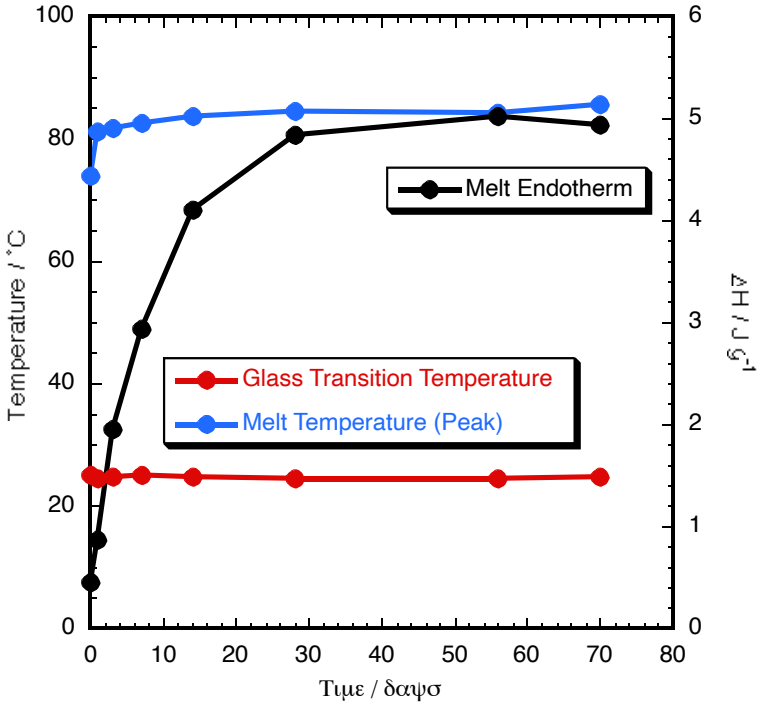

Figure 46. Summary of T_g, Tm and melt endotherm for billet material annealed at 40˚C.

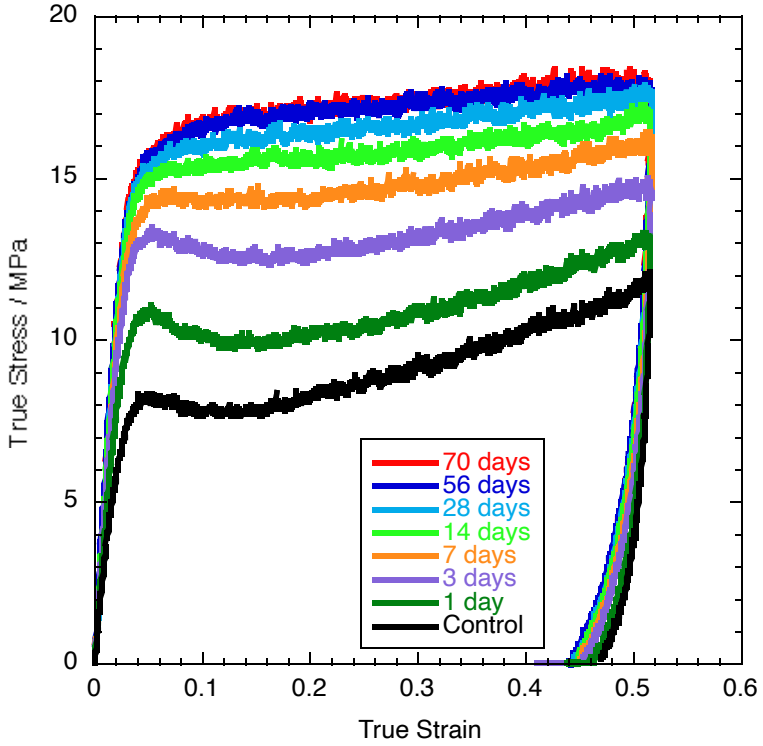

Figure 47. Compression response at 21˚C of billet material annealed at 40˚C.

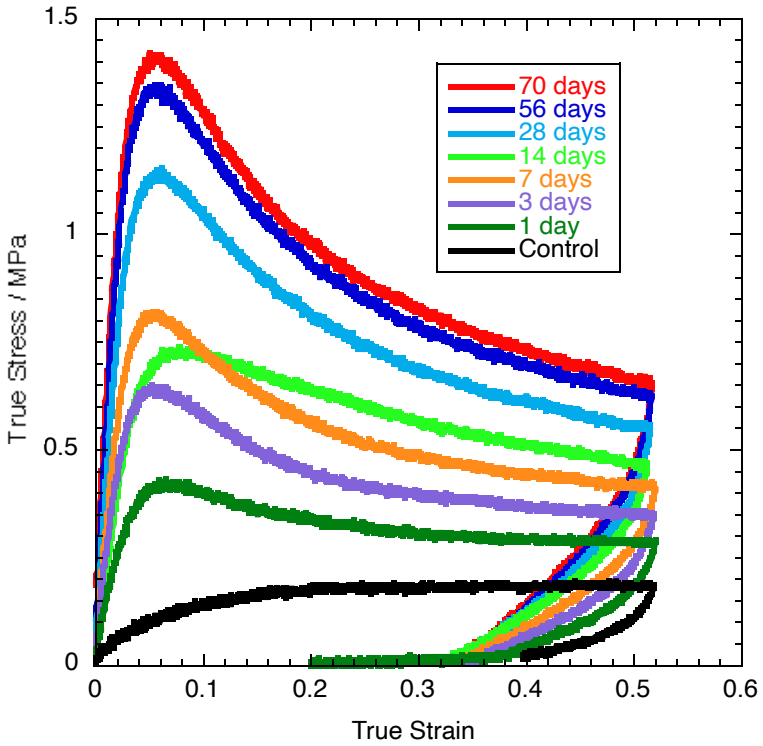

Figure 49. Compression response at 70˚C of billet material annealed at 40˚C.

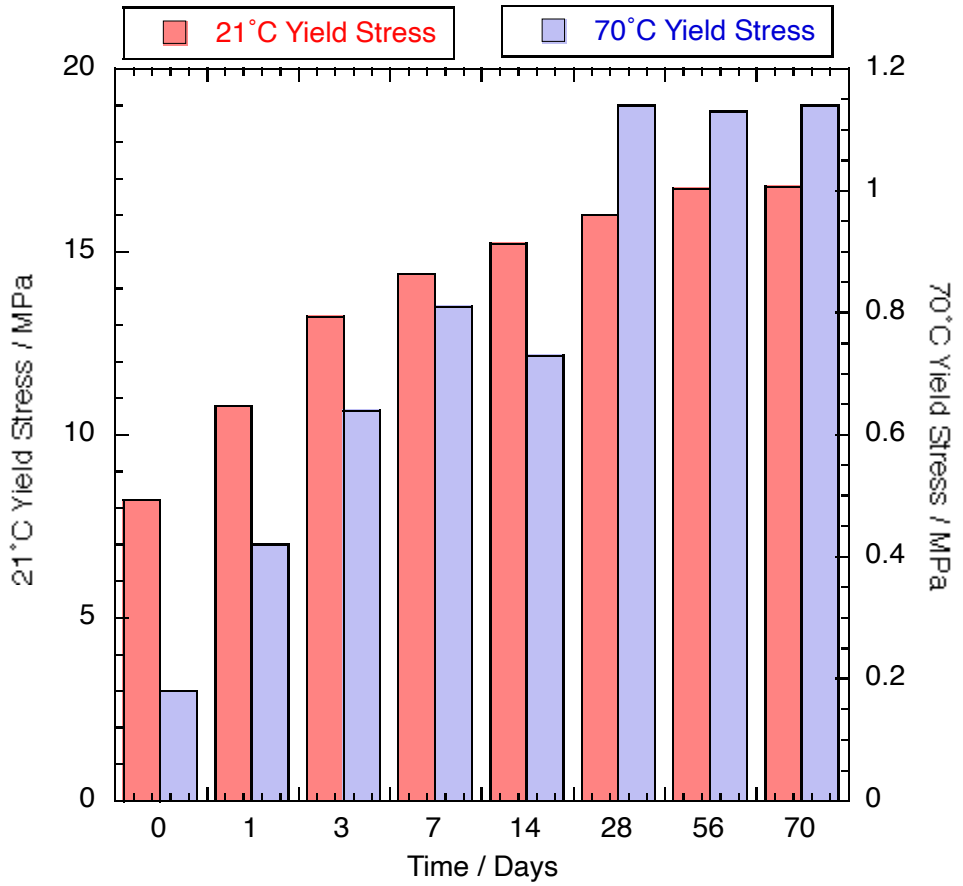

Figure 50. Summary graph of yield stress vs. annealing time for billet material annealed at 40˚C.

New Production Material (LOT 1) Results

The curves obtained from DSC analysis of three different samples of Kel-F 800 are shown in figure 51. The glass transition temperatures of all samples are similar at around 26˚C, however the peak melting temperature increases slightly with increasing crystallinity. This is due to increasing crystal perfection as well as percentage, requiring greater energy to initiate melting. Apart from the obvious differences in the area under the melt endotherm, all three samples exhibit the same general features.

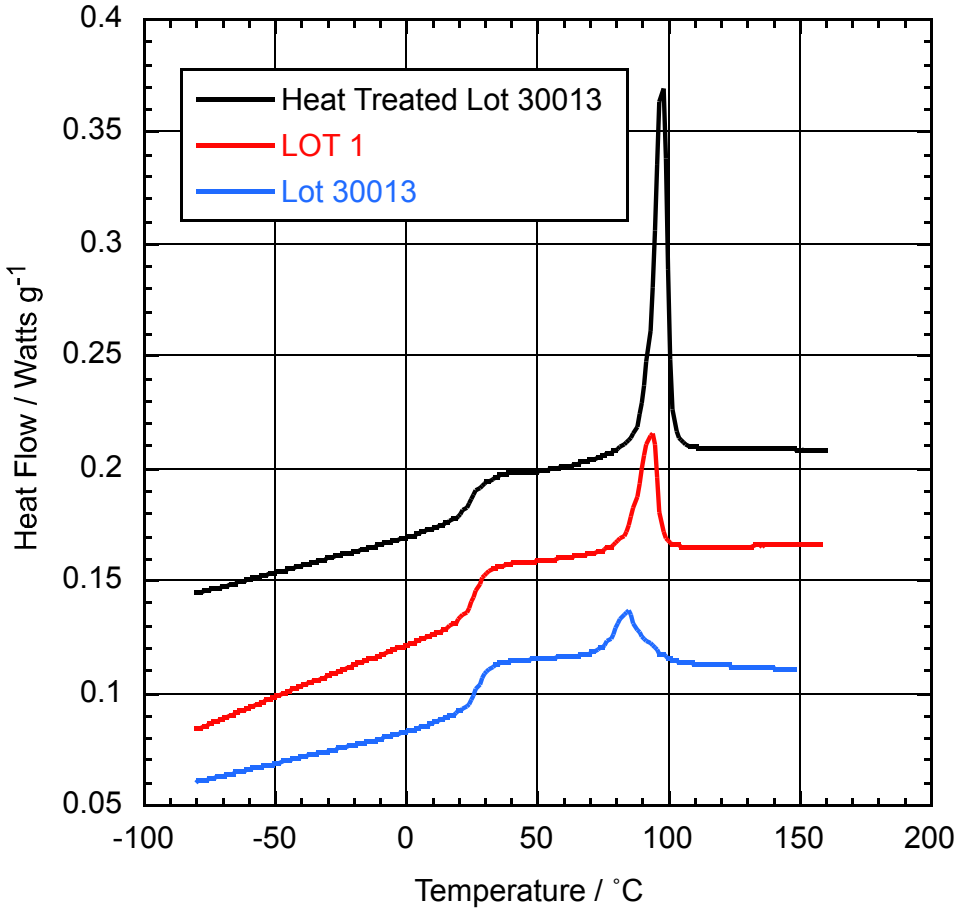

Figure 51. Three DSC curves of different Kel-F 800 lots and thermal treatments. The as received 30013 lot has an approximate crystallinity of 5%, after 68 days at 65˚C this increased to 16.5%. LOT 1 material has a crystallinity of 7.4%. Note. Curves were shifted on the y-axis to improve visual discrimination.

The material response measured by DMA is shown in figure 52 at four different frequencies. From the tan-delta curves two relaxations can be seen, one at approximately 30-40˚C corresponds to the T_g Another broader relaxation is centered at approximately -60˚C. As with most polymers, the measured T_g is a function of frequency (strain-rate), with increasing rate appearing to raise T_g. The change in mechanical response associated with the glass transition can be seen to be more abrupt at lower strain-rates. The upward gradient seen in the tan delta curves below -130˚C is probably an experimental artifact

from the extremely low temperatures causing slight initial grip slippage. It is not thought to represent the onset of a third relaxation.

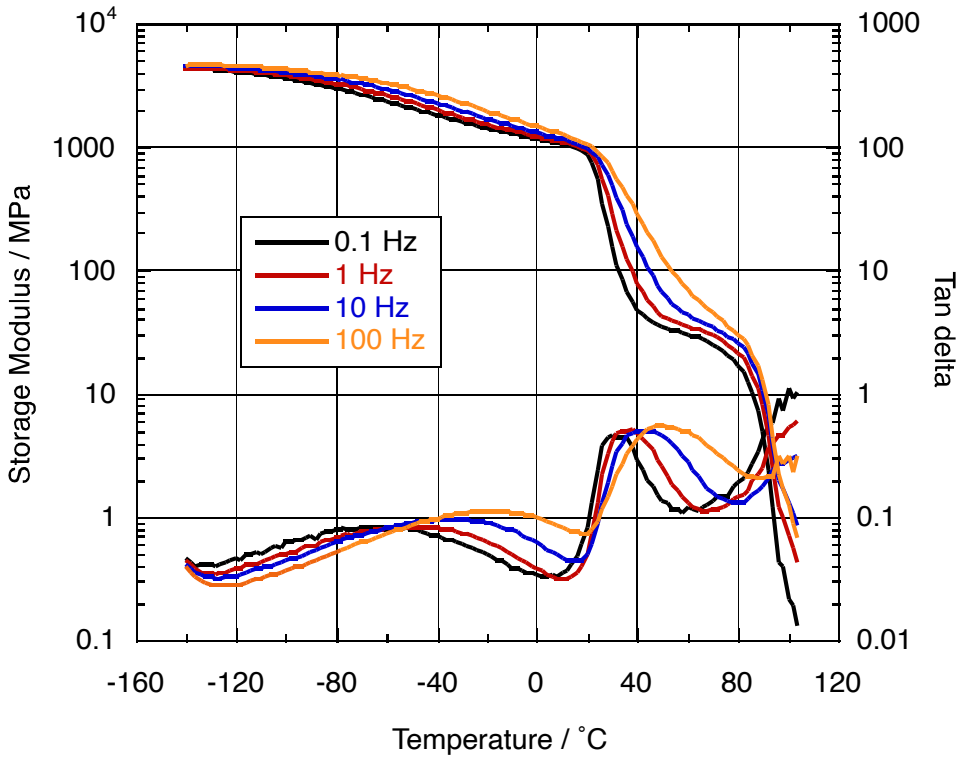

Figure 52. The mechanical response of LOT 1 Kel-F 800 measured by DMA at four frequencies.

The compressive response as a function of temperature of the LOT 1 material is shown in figure 53. Owing to the large change in properties with temperature, a logarithmic stress axis is required to show all the data clearly. It will be seen that at all temperatures except 70˚C the material showed little if any work hardening out a strain of 50%. At 70˚C the material strain softens, this may be related to onset of crystalline domain melting. DSC traces of this material show that the main melt occurs at 94˚C, however the onset of the melt endotherm can be seen to occur from approximately 70˚C when scanned at 10˚C min^{-1}. The glass transition temperature (T_g) from DSC measurements is at 26.5˚C. This is reflected in the large drop in flow stress measured at temperatures greater than this temperature. The material also relaxes back further above T_g indicating a more rubbery response.

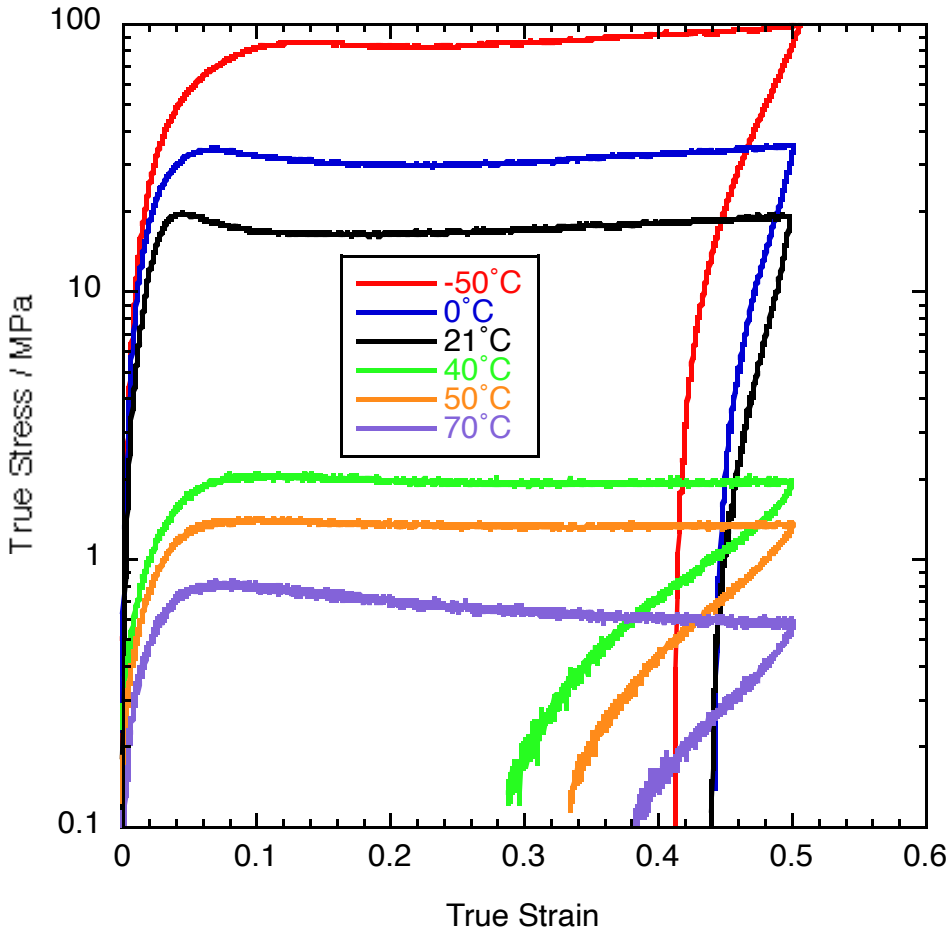

Figure 53. The compressive response of LOT1 Kel-F 800 as a function of temperature (1×10^{-3} s^{-1}).

The compressive response from a strain-rate of 1×10^{-3} s^{-1} to 1 s^{-1} is shown in figure 54. The yield stress is found to be a strong function of strain-rate and a post yield drop is observed in all cases before slight strain hardening. It was seen in figure 53 that this yield drop behavior was only significant at temperatures of 0 and 21˚C with a slight drop at -50˚C. It will also be seen that the loading modulus is a slight function of strain-rate with stiffer response at higher rates.

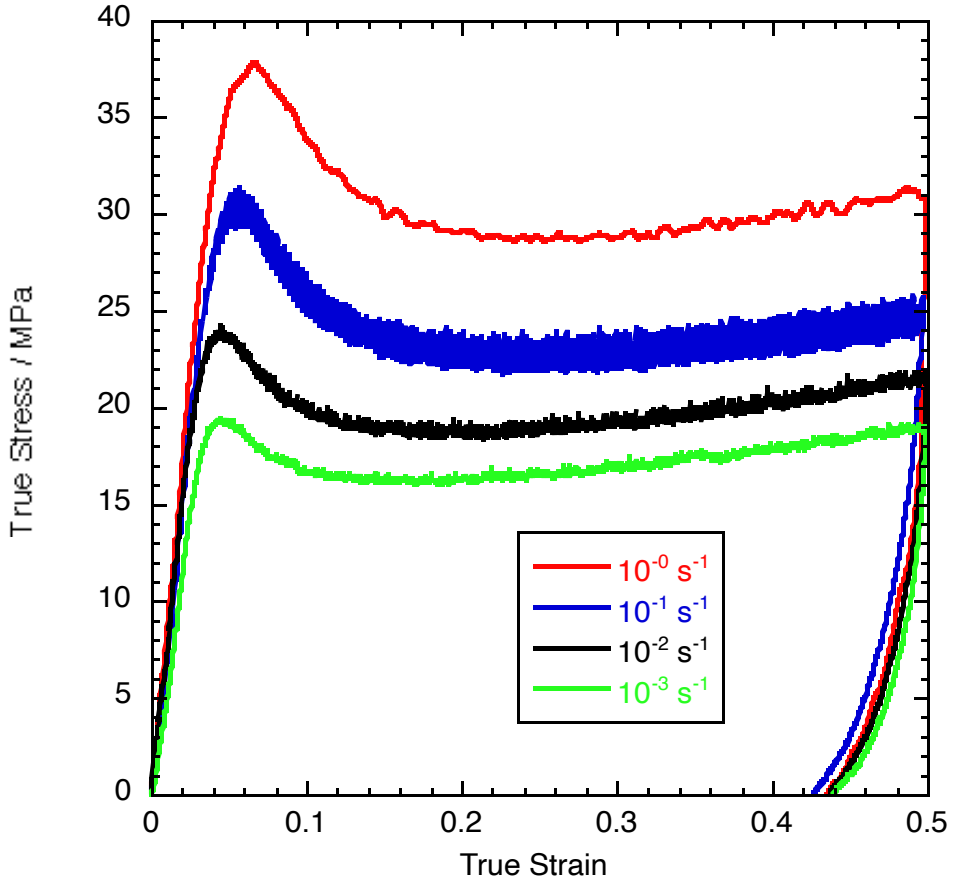

Figure 54. The compressive response of LOT1 Kel-F 800 as a function of strain-rate (21˚C).

Figure 55 shows the effect of temperature on the tensile response. As before, the flow stress is a strong function of temperature and an abrupt reduction in strength is observed above T_g. Below 40˚C the samples were pulled to fracture with the strain to failure increasing with increasing temperature. At 40 and 50˚C the samples did not fracture before the maximum observable engineering strain of 700%. Below T_g a significant yield drop is observed before work hardening commences.

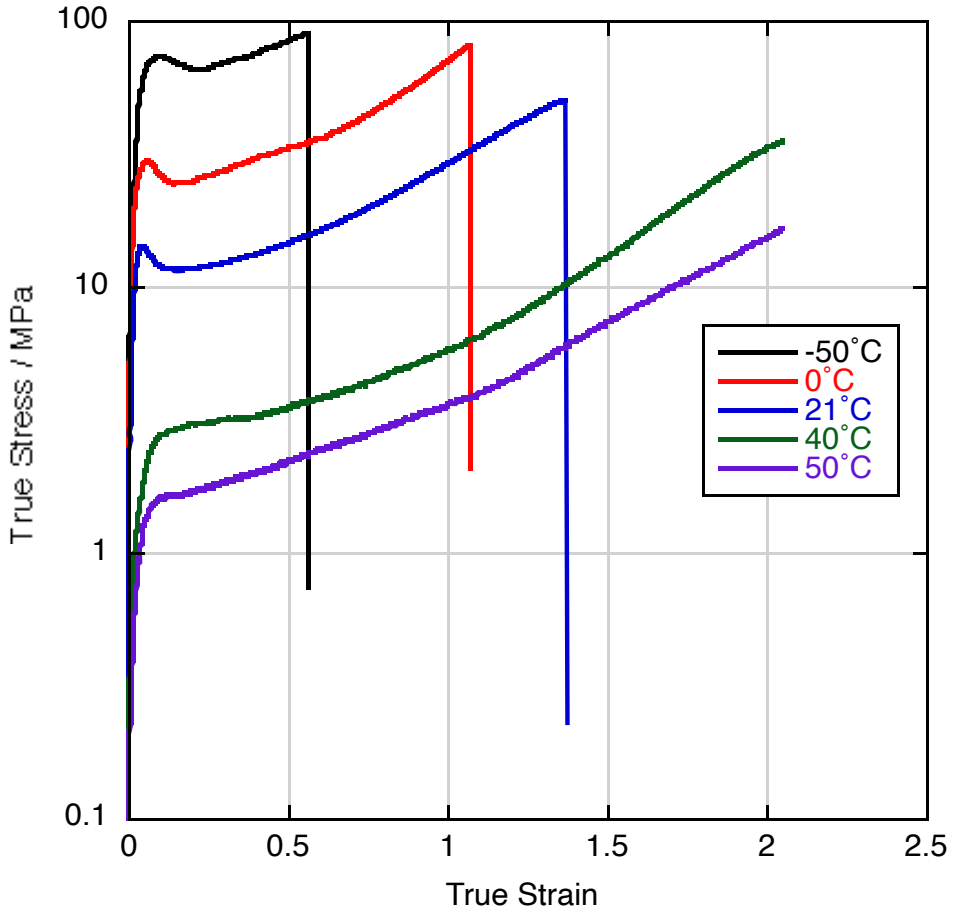

Figure 55. The tensile response of LOT1 Kel-F 800 as a function of temperature (5×10^{-3} s^{-1}). At 40 and 50˚C the tests were stopped before sample failure at an engineering strain of 700%.

Samples from the as received billet of lot 30013 old process Kel-F~800 have been previously compared with the same material that has had the crystallinity increased by thermal conditioning. The crystallinity of the received billet was measured to be 5.0% and the high crystallinity (HC) was measured to be 13% after heating the material to 40˚C for 88 days. The compressive response comparison is shown in figure 56. At -50˚C, well below T_g, the response is seen to be essentially identical, while at the start of melting in some crystal domains (70˚C), the higher crystallinity polymer has a significantly higher flow stress.

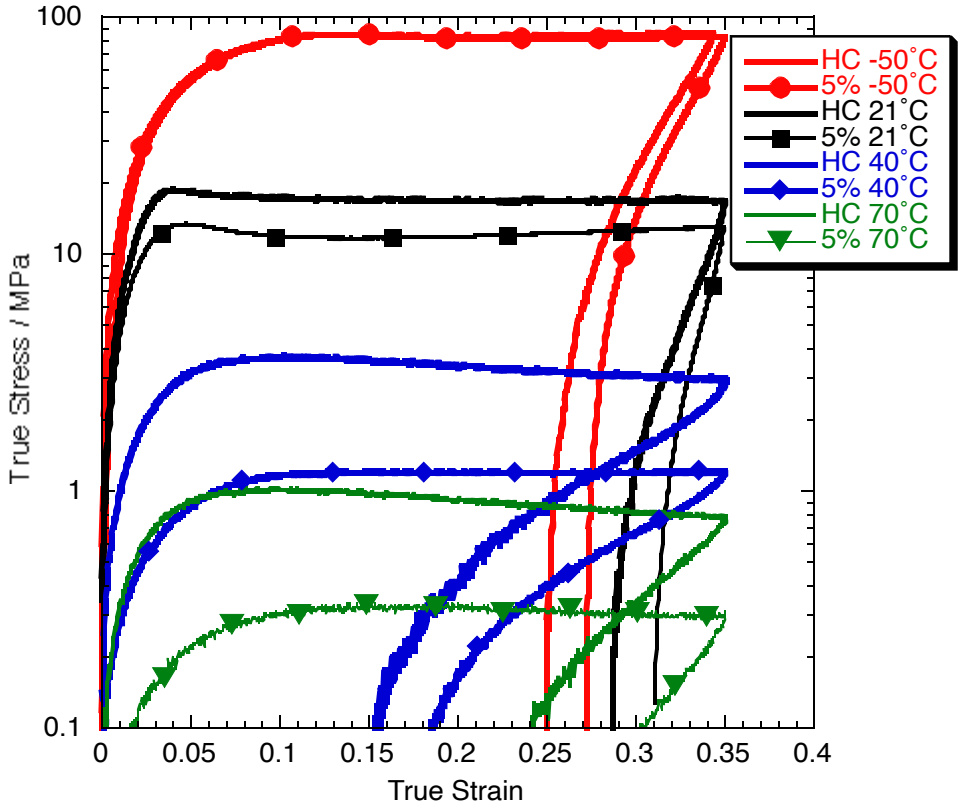

Figure 56. The compressive response of two crystallinities of Lot 30013 Kel-F 800 as a function of temperature (1×10^{-3} s^{-1})

The material response measured by DMA of Lot 30013 Kel-F~800 is shown in figure 57 at four different frequencies. The same general trends seen in figure 52 are seen with a relaxation associated with T_g and a second broad relaxation at approximately -60˚C. For comparison, the DMA response at 10 Hz of the two lots is shown in figure 58. With the exception of the probable experimental artifact in the LOT 1 material below -130˚C, the curves show excellent reproducibility. Above 60˚C some deviation occurs, but this is around the onset of crystalline melting and differences would be expected in the response owing to the small variation in crystallinity between the two different billets.

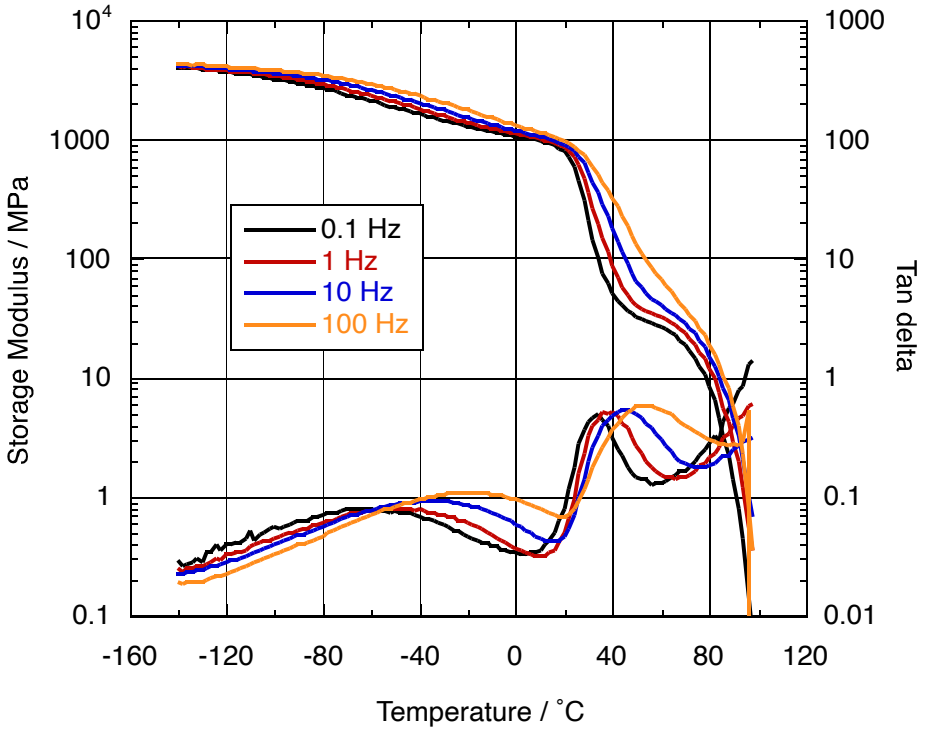

Figure 57. The mechanical response of Lot 30013 Kel-F˚800 measured by DMA at four frequencies.

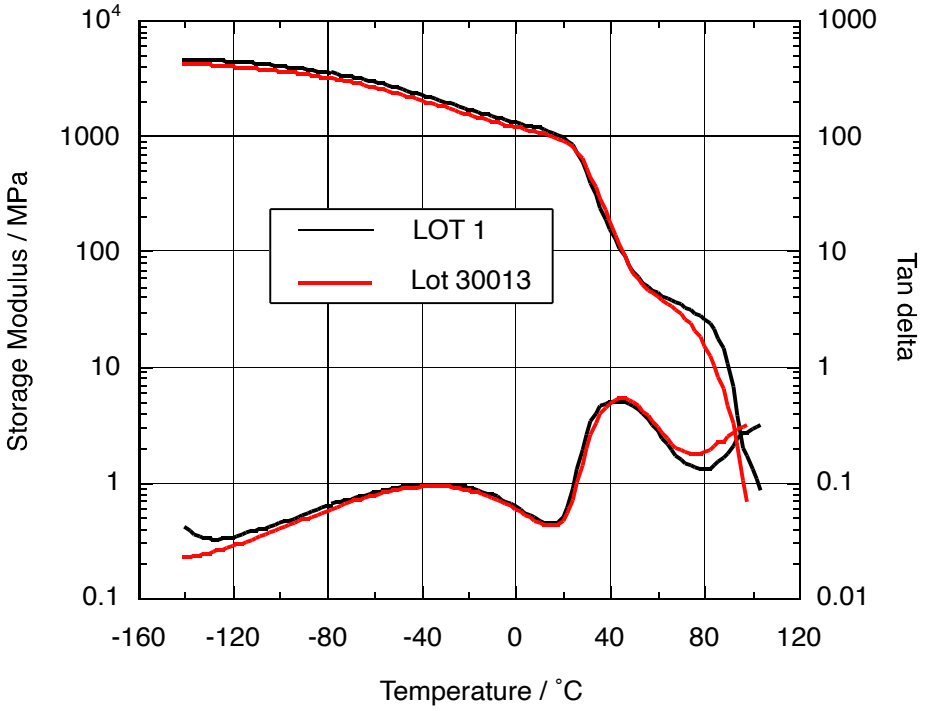

Figure_58. A comparison of the 10˚Hz DMA response of LOT 1 and Lot 30013 Kel-F 800.

Thermogravimetric Analysis (TGA) continually measures the mass of a material sample as it is heated and begins to break down. A steady gas purge removes the breakdown gas products from the weighing pan. Figure 59 shows the mass loss of both new and old lots of Kel-F~800 in air and nitrogen gas purges. As expected significant breakdown occurs at a slightly lower temperature in air than nitrogen owing to the oxygenation processes available. Both lots of material show excellent reproducibility in thermal breakdown response.

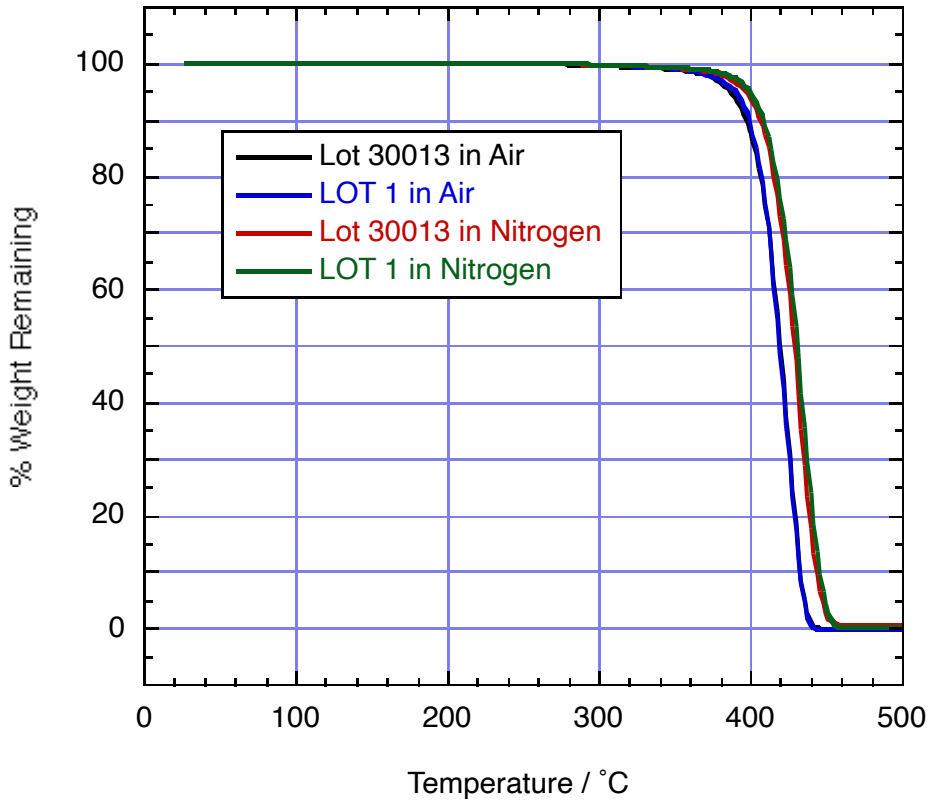

Figure 59. TGA response of LOT 1 and Lot 30013 Kel-F 800.

For comparison, the compressive data for LOT 1 material are plotted along side the 5.0% lot 30013 material in figure 60. As before the response at -50˚C is seen to be identical while at higher temperatures, above T_g, the higher crystallinity material (LOT1 7.4%) has a higher flow stress. The magnitude of the flow stress difference is less than in figure 56 but then the change in crystallinity magnitude is also lower.

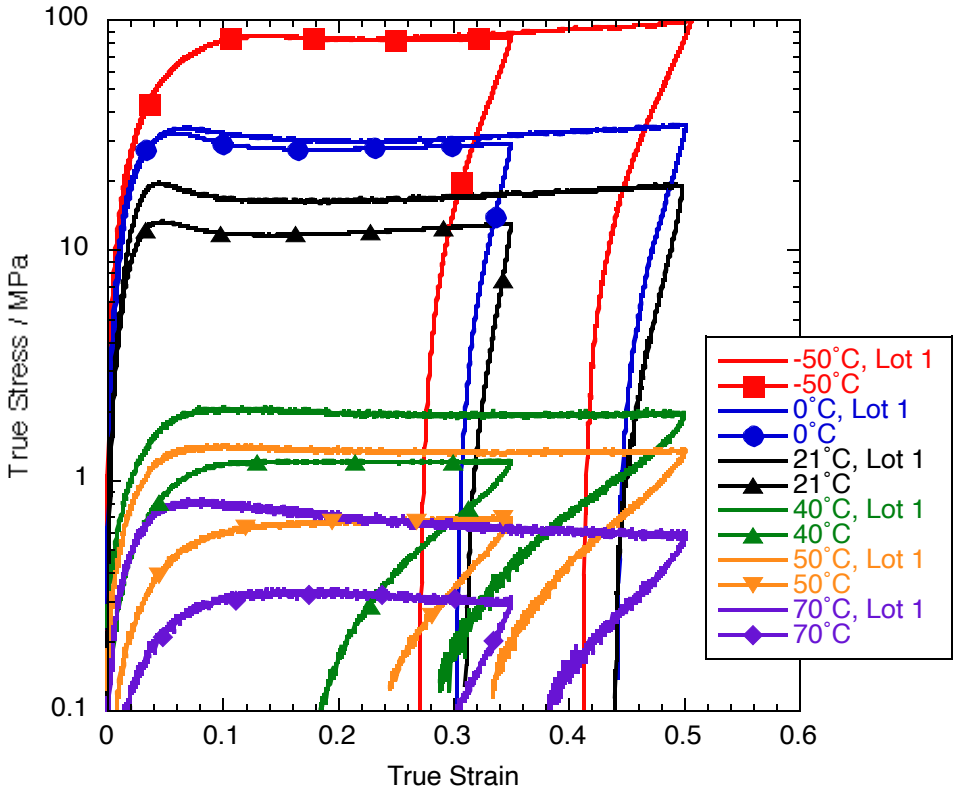

Figure 60. The compressive response of Lot 30013 and LOT1 Kel-F~800 as a function of temperature (1×10^{-3} s^{-1}).

Finally, figure 61 shows a comparison of the tensile response of the LOT1 and lot 30013 material with respect to temperature. A similar trend to before is revealed with the plots significantly below T_g being very similar but some deviation occurring at higher temperatures. The magnitude of this deviation above T_g is smaller than in compression. Additionally, from the low number of tests performed, no differences in the strain to failure can be seen between the two batches.

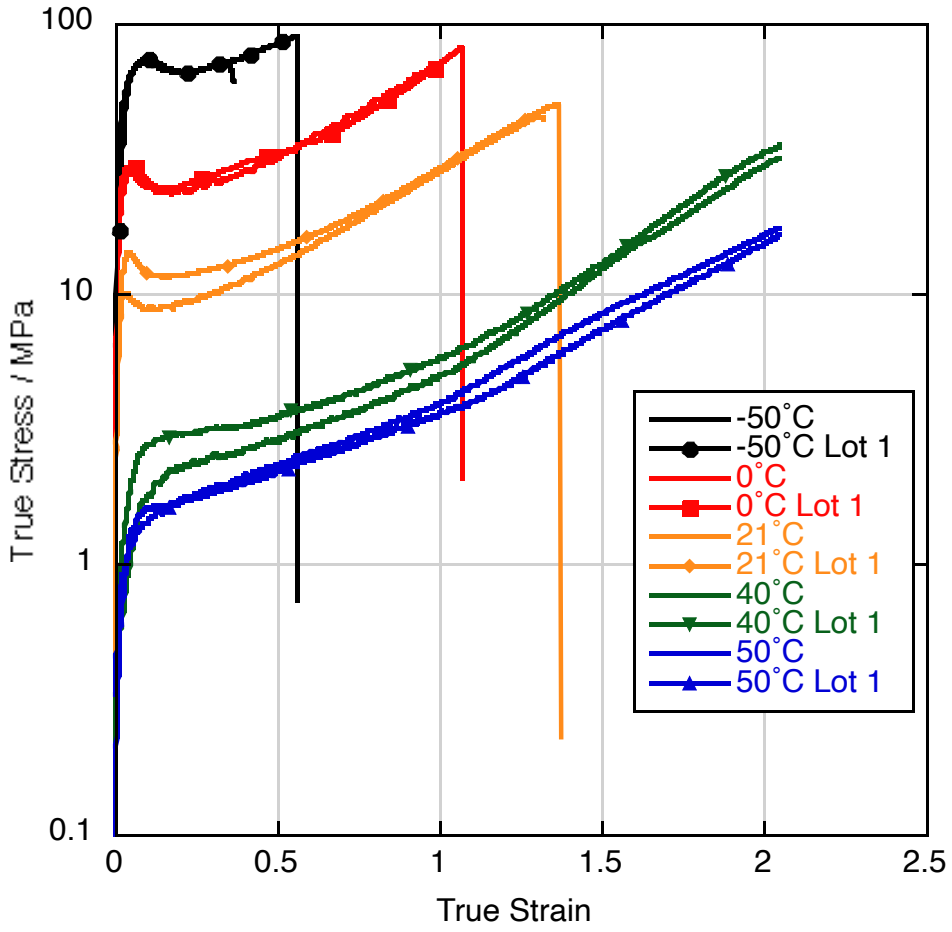

Figure 61. The tensile response of Lot 30013 and LOT1 Kel-F~800 as a function of temperature (5×10^{-3} s^{-1}). At 40 and 50˚C the tests were stopped before sample failure at an engineering strain of 700%.

Compressive Post Yield Drop Investigation

As previously discussed, Kel-F 800 exhibits a post yield drop in stress when tested at room temperature and at strain-rates above 1×10^{-4} s^{-1}. An investigation was made to try to learn more about this phenomenon. Figure 62 shows stress vs. strain curves for a cylindrical sample that was loaded twice. The first strain increment was 0.1 after waiting 5 minutes the relaxed sample length was measured again prior a second loading to a strain of 0.3. Since the curves line up to form a continuous 'single' loading curve, it is clear that in 5 minutes the material has not had a chance to recover. Figure 63 shows a similar result for material deformed twice to a strain of 0.2 with a 5 minute pause. In this case a slight post yield drop is noted prior to resuming the regular curve, however the reload yield is not of the same magnitude as un-deformed material. In figure 64 the result of waiting 1 month before reloading is shown. In this case, the material has recovered to a yield stress similar to the un-deformed material, but the large strain behavior appears unaffected. This is reflected by the present of a second post yield drop in the reloaded material

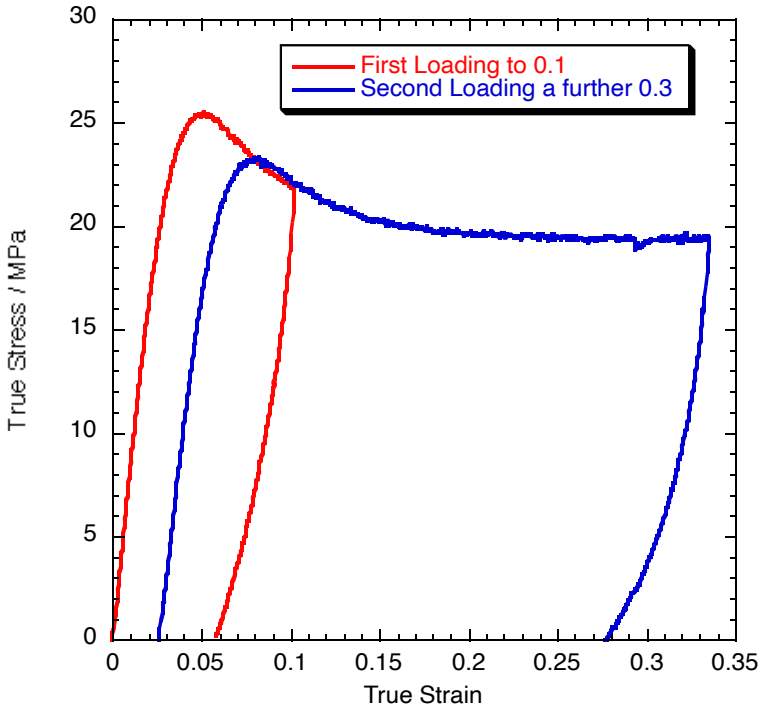

Figure 62. Reloading behavior after a 5 minute relaxation time under no external stress (21˚C, 1×10^{-1} s^{-1}).

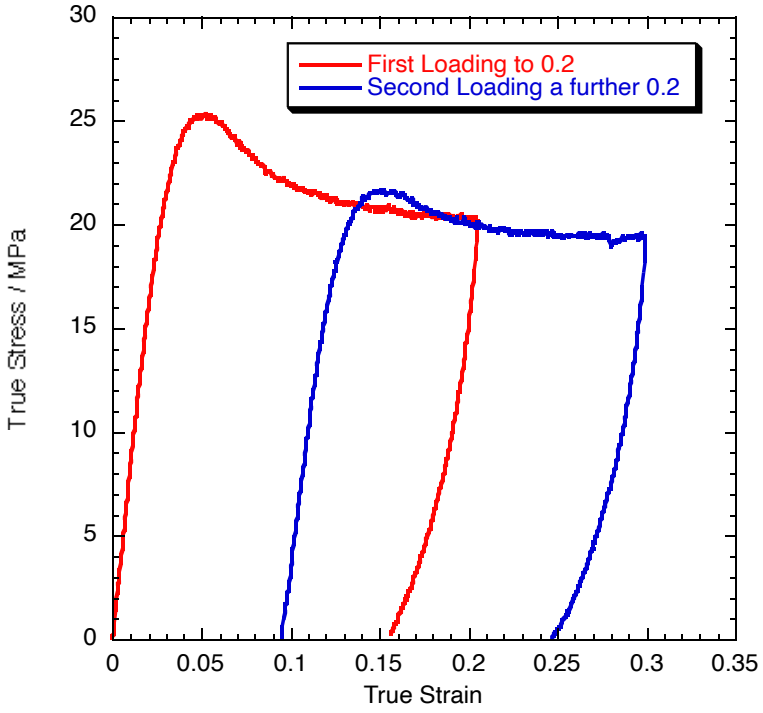

Figure 63. Reloading behavior after a 5 minute relaxation time under no external stress (21˚C, 1×10^{-1} s^{-1}).

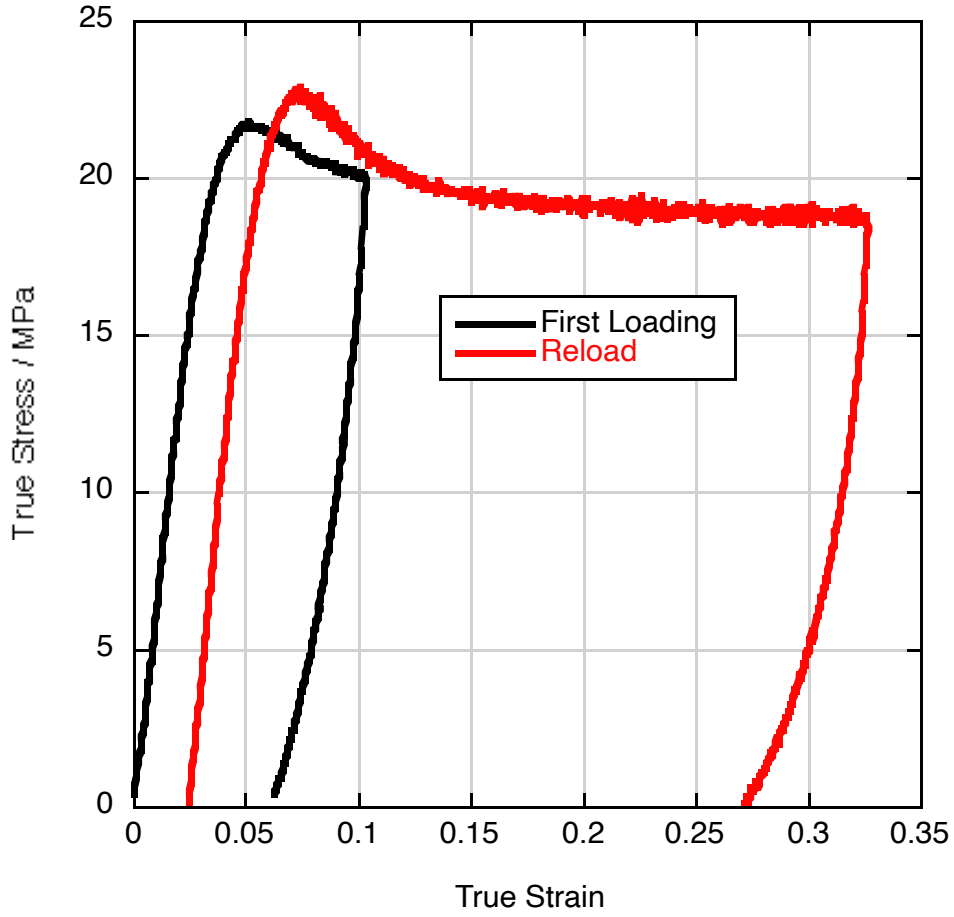

Figure 64. Reloading behavior after a 1 month relaxation time at room temperature (tested at 21˚C, 1×10^{-1} s^{-1}).

To investigate any anisotropic texture developed in Kel-F 800 under compression two cubes were loaded (figure 65). In one case, further deformation was introduced in the original direction after re-machining the sample. In the other sample, the reload was applied perpendicular to the original direction to see if the tensile strain developed by the Poisson effect influenced the compressive behavior. This may also be considered an investigation of the Bausinger effect. The perpendicular loaded sample curve was shifted in strain by the residual strain from the first loading ignoring the direction change. The response in each case was similar with the time taken for re-machining of the sample (approximately 3 hours) not allowing the material to regain full strength. Since the perpendicular loading was not influenced by the previous tensile strain, it appears that Kel-F 800 does not exhibit a Bausinger effect under these conditions.

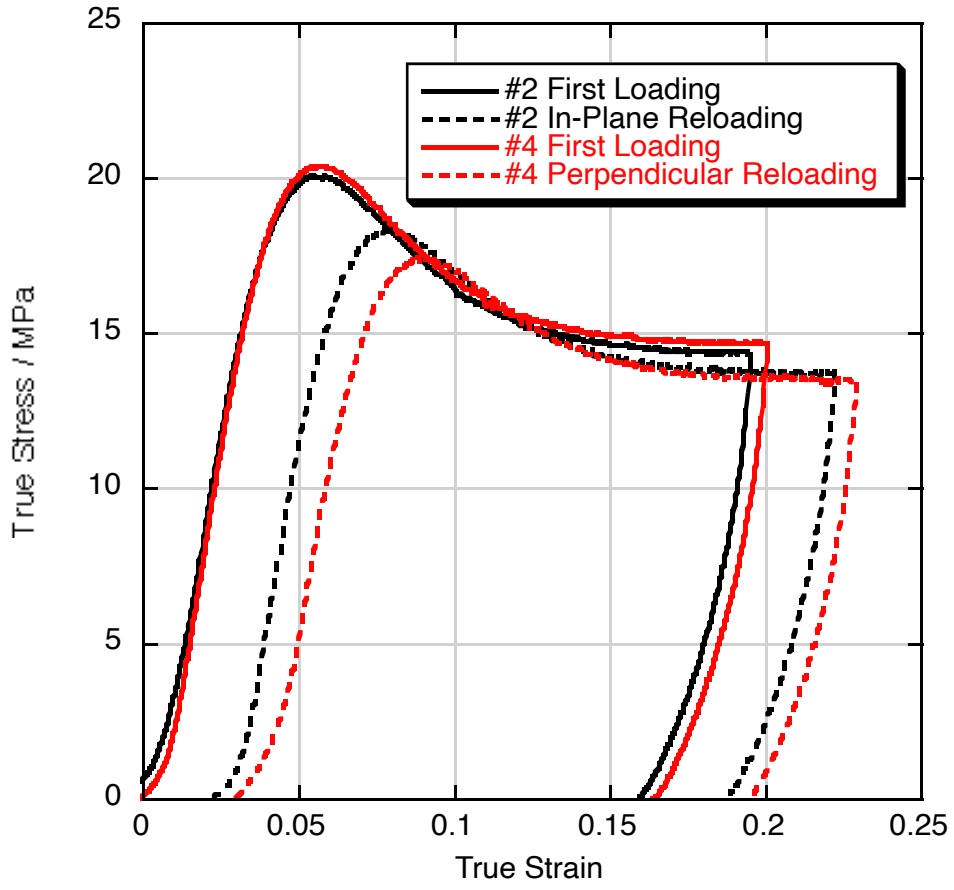

Figure 65. Repeat loading of two Kel-F 800 cubes strained uniaxially and perpendicularly to the original direction (21˚C, 1×10^{-1} s^{-1}).

Ultrasonic sound speed measurements

The speed of sound in PEEK was measured using a time of flight method [11]. Room temperature samples 12 mm thick were tested using longitudinal (C_l) and shear wave (C_s) inducing heads. Suitably correcting for triggering and coupling medium delays, the results are shown in table 1. Values for Young's modulus, Poisson ratio, shear modulus and bulk modulus were calculated using the sound speeds and measured density (ρ). This assumes an isotropic material and that the minute strains imposed on the sample results in the material behaving in a linear elastic manner.

Counter intuitively, the higher crystallinity materials have lower sound speeds than the amorphous material. This is reflected in the lower calculated shear and Young's modulus, however the bulk modulus and Poisson ratio increase with greater crystallinity as intuition would suggest.

Table 1. The measured sound speeds for Kel-F 800 at three crystallinity values and the corresponding calculated small strain elastic constants.

Property	0%	5%	13%
Longitudinal wavespeed / m s^{-1}	1750±20	1720±10	1710±10
Shear wavespeed / m s^{-1}	740±20	690±10	650±10
Density / kg m^{-3}	1990±1	2006±1	2022±1
Young's modulus / GPa	3.03	2.68	2.42
Shear modulus / GPa	1.09	0.96	0.85
Bulk modulus / GPa	4.64	4.66	4.77
Poisson ratio	0.39	0.40	0.42

Taylor Impact Response

Samples were impacted at a range of velocities and three temperatures. Figure 66 shows three recovered cylinders impacted at room temperature. It will be seen that at 108 m s^{-1} the onset of cracking is just visible in the end of the rod as a small misty patch. At 196 m s^{-1} a single crack has reached the periphery of the sample and at 256 m s^{-1}extensive cracking has occurred at the end of the rod. This gradual increase of damage with increasing velocity is as expected from ones intuitive understanding of the likely response.

Figure 67 shows a selection of recovered rods shot at 0, 22 and 40˚C. The shock and strain heating in these experiments only accounts for about a 10˚C increase in material temperature at the end of the rod. Therefore, the 0˚C rods should remain below the glass transition temperature while the 22 and 40˚C rods are in the range of T_g owing to the large strain-rates imposed in these experiments (10^4-10^5 s^{-1}). It will be seen that the damage scales as the temperature response would predict. At 0˚C and 192 m s^{-1} extensive cracking has occurred while at a slightly higher velocity (212 m s^{-1}) and 40˚C only internal cracking has been caused. At velocities around 300 m s^{-1} extensive shattering of the 0˚C rod has occurred with much more ductile damage occurring at 40˚C.

Finally, figure 68 shows more clearly the difference in incipient damage caused at room and 0˚C at similar velocities.

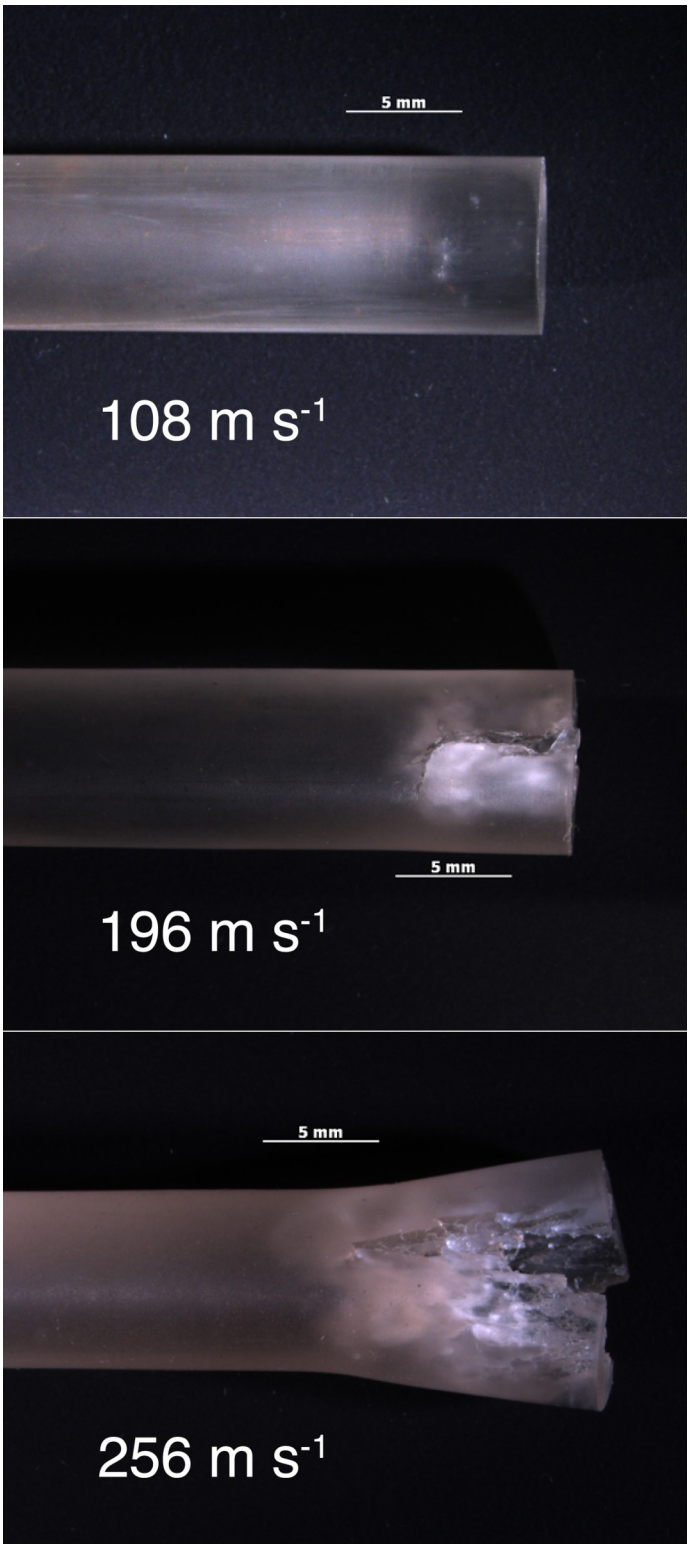

Figure 66. The room temperature (22˚C) response of Kel-F 800 as a function of impact velocity.

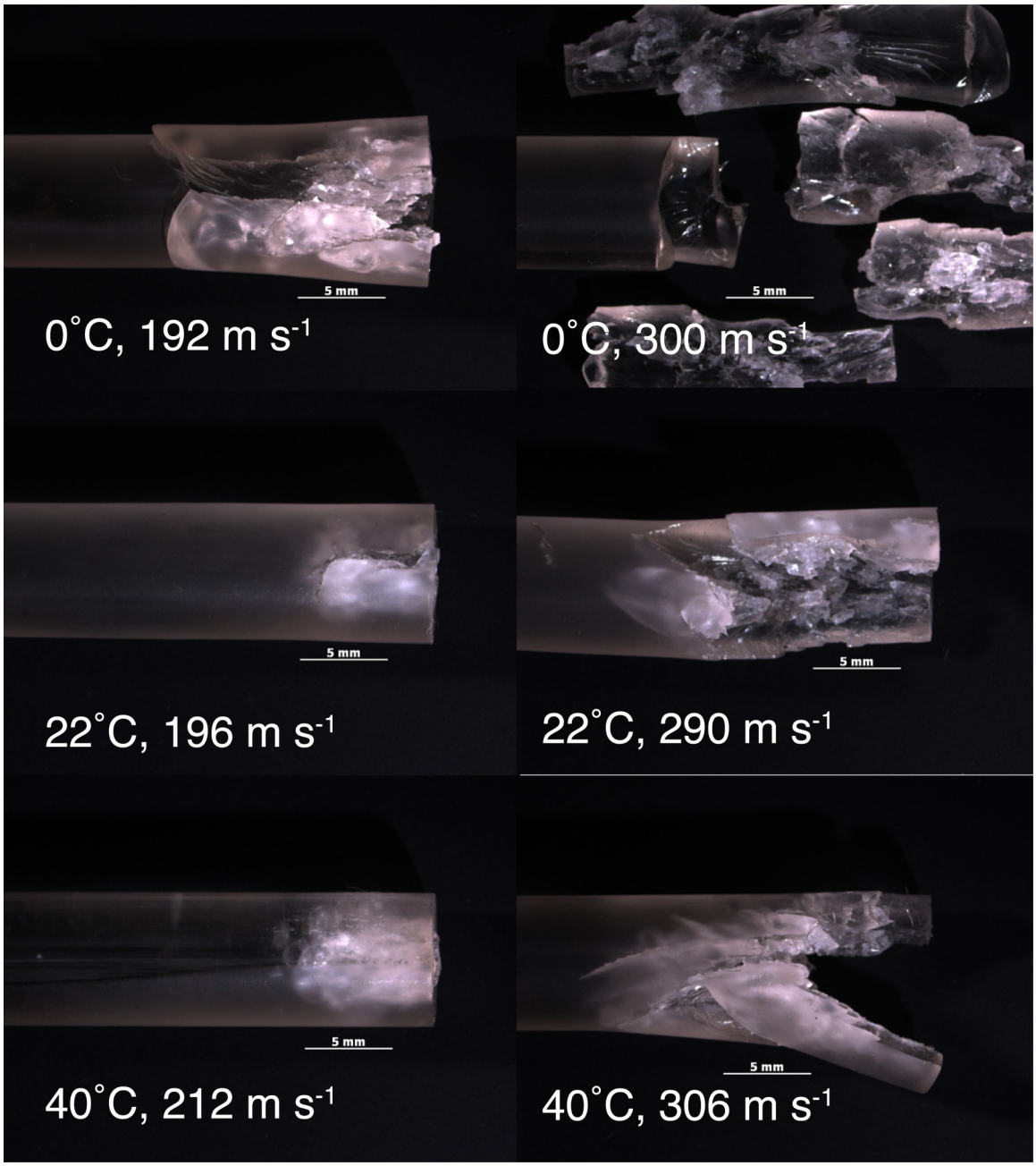

Figure 67. The temperature related Taylor Impact response at various velocities.

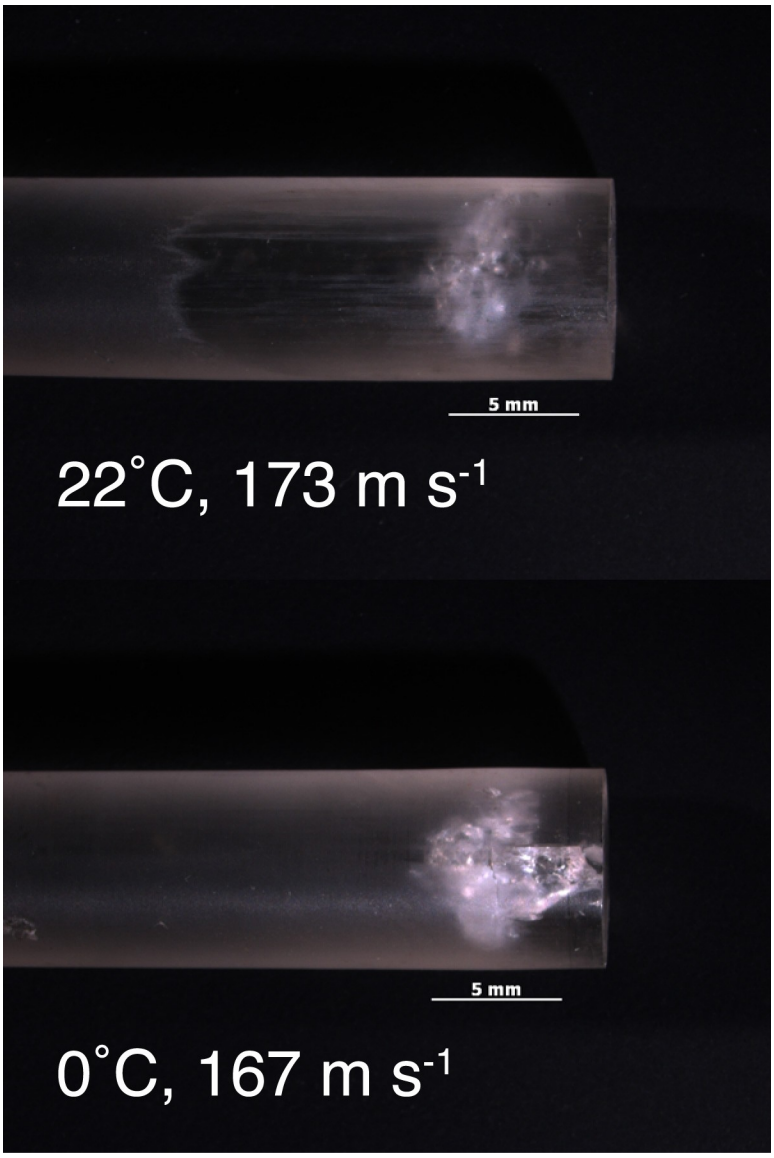

Figure 68. The onset of cracking after Taylor Impact at two temperatures and comparable velocities.

Conclusions

In common with most polymers, the mechanical properties of Kel-F 800 are a strong function of temperature and strain-rate. The properties are also markedly different above and below T_g. Experiments suggest that PBXs made with Kel-F 800 will have approximately 5% crystallinity after manufacture rising to approximately 12% in returned stockpile material. The exact values will depend to some extent on the molecular weight of the Kel-F 800 batch used.

All the materials tested showed a similar flow stress in compression at -50˚C (well below T_g) irrespective of crystallinity. At room temperature a marked drop in stress after yielding before subsequent strain-hardening was observed in low crystallinity

materials. In contrast, high crystallinity materials showed continuous strain-softening after the post-yield drop at higher strain-rates and above T_g. Essentially amorphous Kel-F 800 had an extremely low flow stress above T_g behaving almost as a viscous fluid rather than a visco-elastic solid. In tension, low crystallinity material exhibited great ductility close to and above T_g with a generalized drawing behavior. In contrast, high crystallinity material exhibited a rapid localization after reaching the yield stress at temperatures both above and below room temperature. The total ductility was greatly reduced. At room temperature, the localization could work harden sufficiently quickly that the necked down region would eventually draw out to the full gauge length prior to failure.

The crystallization behavior because of thermal annealing was found to be extremely sensitive to the starting crystallinity of the material. Clearly, the existing crystalline domain nucleation sites are beneficial to subsequent growth. Crystallinity is found to increase with time at an annealing temperature of only 30˚C. This is only slightly above the measured glass transition temperature. The maximum crystallinity achievable from annealing increased with increasing annealing temperature up the highest temperature investigated, 65˚C.

The room temperature post-yield stress drop must involve a structural rearrangement that can recover with extended periods at room temperature. This was demonstrated by undertaking repeat loading tests on samples after 5 minutes and 1-month relaxation times. The post-yield drop effect was only evident in the 1-month sample. Loading in two perpendicular directions was tried to observe any Bausinger type behavior. Since the perpendicular response was essentially identical to a sample loaded only in a single direction, it appears that Kel-F 800 does not exhibit a Bausinger effect.

Sound speeds were measured in Kel-F 800 material of three crystallinities. Strangely, the sounds speeds decreased slightly with increasing crystallinity. Therefore, the calculated Young's modulus also decreased with increasing crystallinity. These effects may just be a function of the greater density measured in higher crystallinity samples. The calculated bulk modulus did increase with increasing crystallinity.

The analysis of Taylor impact samples of 5% crytallinity Kel-F 800 showed intuitive results. The increasing damage at a constant starting temperature was found to scale with increasing impact velocity. Samples impacted at an approximately constant velocity, but differing temperatures, were found to respond as expected; colder samples exhibited less ductility and greater damage for a given velocity.

No differences in the mechanical and thermal response can be observed between the LOT 1 Kel-F~800 manufactured by the new process and the older production material that cannot be explained by the slight differences in crystallinity between the two billets.

Acknowledgments

Thanks are given to the following people for assistance with various aspects of this research, E. Bruce Orler, Bradford Clements, Eric Brown and Dana Dattelbaum.

References

[1] Cady, W.E. and L.E. Caley, *Properties of Kel-F 800 Polymer*. 1977, Report number UCRL-52301, Lawrence Livermore Laboratory, CA.

[2] Byers, L. and P. Deacon. *Characterisation of FK-800 lot 1 by AWE, Aldermaston, UK.* in Summary of LANL-3M Knowledge Capture Discussions, October 16-18. 2006. Minneapolis, MN.

[3] Hoffman, D.M. and S.C. DePiero, *Characterization and Quantification of new TATB and Kel-F 800 for LX-17*. 2007, Lawrence Livermore National Laboratory.

[4] Hoffman, D.M., F.M. Matthews, and C.O. Pruneda, *Dynamic Mechanical and Thermal Analysis of Crystallinity Development in Kel-F 800 and TATB/Kel-F 800 Plastic Bonded Explosives. Part I. Kel-F 800.* Thermochimica Acta, 1989. 156: p. 365-372.

[5] Walley, S.M., et al., *A Study of the Rapid Deformation Behaviour of a Range of Polymers.* Philosophical Transactions of the Royal society of London, 1989. A 328: p. 1-33.

[6] Walley, S.M., et al., *The Rapid Deformation Behaviour of Various Polymers.* Journal de Physique III, 1991. 1(12): p. 1889-1925.

[7] Gray III, G.T. and W.R. Blumenthal, *Split-Hopkinson pressure bar testing of soft materials,* in ASM Handbook, Volume 8, Mechanical Testing and Evaluation, ASM-Handbook-committee, Editor. 2000, ASM International. p. 488-496.

[8] Rae, P.J., et al., *Pressure induced phase change in poly(tetrafluoroethylene) at modest impact velocities.* J. Appl. Phy., 2005. 98(6): p. 1-8.

[9] Rae, P. and E. Brown, *The mechanical properties of poly(ether-ether-ketone) (PEEK) with emphasis on the large compressive strain response.* Polymer, 2007. 48(2): p. 598-615.

[10] Rae, P., E. Brown, and E. Orler, *The influence of temperature and strain rate on the constitutive and damage responses of Polychlorotrifluoroethylene (PCTFE, Kel-F 81)*. Polymer, 2006. 47(21): p. 7506-7518.

[11] Panametrics, Ultrasonic Technical Notes. 2001, www.panametrics.com: Houston, Texas. p. 32-40.